GREEN SYNTHESIS AND CHARACTERIZATION OF ZINC OXIDE NANOPARTICLES USING AQUEOUS BARK EXTRACT OF MALAYAN CHERRY (*Muntingia calabura*)

By

CHUNG JIA MIN

A project report submitted to the Department of Chemical Science

Faculty of Science

Universiti Tunku Abdul Rahman

in partial fulfilment of the requirements for the degree of

Bachelor of Science (Honours) Chemistry

MAY 2024

ABSTRACT

GREEN SYNTHESIS AND CHARACTERIZATION OF ZINC OXIDE NANOPARTICLES USING AQUEOUS BARK EXTRACT OF MALAYAN CHERRY (*Muntingia calabura*)

CHUNG JIA MIN

Zinc oxide nanoparticles (ZnO NPs) were synthesized and characterized through the green synthesis pathway using the bark extract of *Muntingia calabura* with zinc nitrate hexahydrate as the salt precursor and deionized water as the green solvent. The phytochemicals found in the bark extract served as the stabilizing and reducing agent in the synthesis of ZnO NPs. The synthesized ZnO NPs were characterized using Fourier Transform Infrared Spectroscopy (FTIR), UV-Visible Spectroscopy (UV-Vis), X-ray Diffraction (XRD), Field Emission Scanning Electron Microscopy (FESEM) and Energy Dispersive X-ray Spectroscopy (EDX). Based on the results of this study, the phytochemicals in the bark extract that involved in the reaction could be observed in the FTIR spectrum. The formation of ZnO NPs could be proved by the presence of Zn-O stretching at the peak 459 cm^{-1} in the spectrum. The UV-Vis spectrum showed that the maximum absorption wavelength of ZnO NPs was 373 nm with a band gap energy of 3.32 eV. XRD revealed that the structural identity of ZnO NPs to be hexagonal wurtzite structure with a crystallite size of 48.90 nm. Based on FESEM results, the morphology of ZnO NPs was found to be spherical shape

with a particle size ranging from 38.0 nm – 71.4 nm. The elemental composition of ZnO NPs was characterized by EDX which proved the presence of zinc and oxygen.

ABSTRAK

SINTESIS HIJAU DAN PERWATAKAN NANOPARTIKEL ZINK OKSIDA DENGAN MENGGUNAKAN EKSTRAK AQUEOUS BATANG KAYU DARIPADA KERUKUP SIAM (*Muntingia calabura*).

Nanopartikel zink oksida (ZnO NPs) telah disintesis dan dicirikan melalui laluan sintesis hijau menggunakan estrak batang kayu *Muntingia calabura* dengan zink nitrat heksahidrat sebagai precursor dan air ternyahion sebagai pelarut hijau. Fitokimia yang terdapat dalam estrak batang kayu berfungsi sebagai agen penstabil dan pengurangan dalam sintesis ZnO NPs. ZnO NPs yang disintesis telah diciri dengan menggunakan Spektroskopi Inframerah Fourier Transform (FTIR), Spektroskopi UV-Visible (UV-Vis), Difraksi Sinar-X (XRD), Mikroskop Elektron Pengimbasan Pelepasan Medan (FESEM) and Analisis Penyebaran Tenaga Sinar-X (EDX). Berdasarkan hasil kajian ini, fitokimia dalam ekstrak kulit batang kayu yang terlibat dalam tindak balas boleh diperhatikan dalam spektrum FTIR. Pembentukan zink oksida boleh dibuktikan dengan kehadiran regangan Zn-O at puncak 459 cm^{-1} dalam spektrum. Selain itu, spektrum UV-Vis menunjukkan bahawa puncak penyerapan maksumum ZnO NPs ialah 373 nm dengan tenaga jurang jalur 3.32 eV. XRD mendedahkan bahawa identiti struktur ZnO adalah struktur wurtzite heksagon dengan saiz kristal 48.90 nm. Berdasarkan Keputusan FESEM, morfologi ZnO NPs didapati berbentuk sfera dengan saiz zarah antara 38.0 nm hingga 71.4 nm. Komposisi

unsur ZnO NPs dicirikan oleh EDX yang membuktikan kehadiran zink dan oksigen.

ACKNOWLEDGEMENT

Throughout my final year project, I would like to express my gratitude to all those who have contributed to my completion of this final year project. Firstly, I would like to thank my supervisor, Dr. Yip Foo Win for his guidance, support and encouragement throughout my project to make sure that I am on the right direction.

I am also thankful UTAR for providing facilities and instruments to facilitate my final year project studies. Next, I sincerely appreciated all UTAR laboratory staffs and officers of Faculty of Science, Mr. Seou Chi Kien, Mr. Chong Boon Rui, and Mr. Leong Thung Lim for their guidance and assistance throughout my studies. Additionally, I am deeply thankful to all lecturers for teaching me in my studies to allow me to leverage the knowledge in my project.

Lastly, I am profoundly thankful to my family and friends for their endless support and understanding throughout my academic journey in UTAR. Without their encouragement and support, I would not have achieve success in this endeavor. Thank you!

DECLARATION

I hereby declare that this final year project report is based on my original work except for quotations and citations which have been duly acknowledged. I also declare that it has not been previously or concurrently submitted for any other degree at UTAR or other institutions.

CHUNG JIA MIN

APPROVAL SHEET

This final year project report entitled "**GREEN SYNTHESIS AND CHARACTERIZATION OF ZINC OXIDE NANOPARTICLES USING AQUEOUS BARK EXTRACT OF MALAYAN CHERRY (*Muntingia calabura*)**" was prepared by CHUNG JIA MIN and submitted as partial fulfilment of the requirements for the degree of Bachelor of Science (Hons) Chemistry at Universiti Tunku Abdul Rahman.

Approved by:

YIP FOO WIN

_____

(Dr. Yip Foo Win) Date: 3 May 2024

Supervisor

Department of Chemical Science

Faculty of Science

Universiti Tunku Abdul Rahman

FACULTY OF SCIENCE

UNIVERSITI TUNKU ABDUL RAHMAN

Date: 2 MAY 2024

PERMISSION SHEET

It is hereby certified that **CHUNG JIA MIN** (ID No: **20ADB02266**) has completed this final year project thesis entitled "GREEN SYNTHESIS AND CHARACTERIZATION OF ZINC OXIDE NANOPARTICLES USING AQUEOUS BARK EXTRACT OF MALAYAN CHERRY (*Muntingia calabura*)" under the supervision of Dr. YIP FOO WIN from the Department of Chemical Science, Faculty of Science.

I hereby give permission to the University to upload the softcopy of my final year project thesis in pdf format into the UTAR Institutional Repository, which may be made accessible to the UTAR community and public.

Yours truly,

CHUNG JIA MIN

TABLE OF CONTENTS

LIST OF TABLES

LIST OF FIGURES

LIST OF SYMBOLS/ABBREVIATIONS

Å	Angstrom
C	Carbon
c	Speed of light
C=O	Carbonyl group
COOH	Carboxylic acid
cm^{-1}	Wavenumber or frequency unit
E_g	Band gap energy
EDX	Energy Dispersive X-ray
eV	Electron volt
e^-	Electron
FESEM	Field Emission Scanning Electron Microscopy
FTIR	Fourier Transform Infrared
FWHM	Full width half maximum
g	Gram
h	Planck's constant
H	Hydrogen
HCl	Hydrochloric acid
hv	Incident photon energy
H_2O	Water molecule
ICDD	International Centre of Diffraction Standard

k	Scherrer’s constant
KBr	Potassium bromide
kV	Kilovolt
M. calabura	*Muntingia calabura*
m	Milli
mg	Milligram
Mg	Magnesium
mL	Millilitre
NO_3^-	Nitrate ion
nm	Nanometre
NPs	Nanoparticles
O	Oxygen
OH	Hydroxyl group
TEM	Transmission Electron Microscopy
UV	Ultraviolet
UV-Vis	Ultraviolet-Visible
W	Watt
XRD	X-ray Diffraction
Zn	Zinc
Zn^0	Metallic zinc
Zn^{2+}	Zinc (II) ion
ZnO	Zinc oxide
ZnO NPs	Zinc oxide nanoparticles
λ	Wavelength
λ_{max}	Maximum wavelength

°	Degree
℃	Degree Celsius
α	Absorption coefficient
β	Full width at half maximum (FWHM) of the diffraction peak in radian 2θ
π	Pi
θ	Bragg's angle of diffraction

CHAPTER 1

INTRODUCTION

1.1 Background of study

The concept of nanotechnology was introduced by Richard Feynman, an American physicist, and Nobel Prize Laureate (Bayda et al., 2019). In 1959, Feynman delivered a talk entitled “There is Plenty of Room at the Bottom” and discussed the potential to manipulate and control matter on a small scale, thereby opening avenues for the field of nanotechnology. Feynman explored the potential for miniaturization and discussed the technology implications of working at atomic and molecular levels. The idea of Feynman was proven to be correct, and he was known as the father of modern technology. Later in the 1974, the first person to define the term “nanotechnology” was a Japanese scientist named Norio Taniguchi. Nanotechnology involves separation, consolidation, and deformation process by one atom or one molecule. The prefix “nano” refers to a Greek prefix meaning something that is extremely tiny. It presents one billionth or 10^{-9} m. Nanotechnology is the utilization of the technology in practical applications to produce nano products that range from 1 – 100 nm (Bayda et al., 2019).

Nanotechnologies are working at the nanoscale and have significant contributions to almost every field of science which include physics, biology and chemistry and engineering. Particles that are produced with a dimension of about 1 – 100 nm are known as nanoparticles. Nanoparticles are totally different from the bulk materials. The chemical and physical properties of nanoparticles such as the size, structure and morphology will be different from their bulk state (National Nanotechnology Initiative, 2022). In recent years, those advance nations such as China, Europe and the United States invest heavily in nanotechnology due to its great potential and benefits in various fields. This is because nanotechnology is more affordable than the traditional methods involving mass bulking and heavy machinery. Furthermore, nanotechnology has a great potential to be applied in all aspects of life, encompassing nanoelectronics, nanomaterials sciences and nanomedicine. Therefore, it is reasonable to believe that nanotechnology will emerge as a mandatory field of study in the future (Malik, Muhammad and Waheed, 2023).

1.2 Nanoparticles

Nanoparticles have various structure, size, and shape such as spherical, cylindrical, hollow core, tubular or irregular (Joudeh and Linke, 2022). Nanoparticles can be classified into organic and inorganic nanoparticles. Organic nanoparticles such as micelles, liposomes, and polymeric nanoparticles, they are biodegradable and non-toxic. Organic nanoparticles are capable to break down naturally, they are light and heat sensitive. These organic nanoparticles are

known as nanocapsules. These organic nanoparticles are useful in the field of pharmaceuticals for transportation purposes. Inorganic nanoparticles do not contain carbon and they are non-toxic (Alshammari et al., 2023). Some of the examples of inorganic nanoparticles are metal nanoparticles, ceramic nanoparticles, and semiconductor nanoparticles (Joudeh and Linke, 2022). Due to the fact that inorganic nanoparticles exhibit greater stability compared to organic nanoparticles, this causes inorganic nanoparticles to be widely used in various field. In addition, nanoparticles can be classified based on different dimension. Dimension is an important property to distinguish various nanoparticle structures. The different types of nanoparticles are classified based on their dimensional as shown in Table 1.1.

Table 1.1: Classification of nanoparticles based on dimension (Abid et al., 2022).

Dimension	Structure
Zero-dimensional (0-D)	• All three dimensions within the nanoscale range. • Examples: nanospheres and nanoclusters,
One-dimensional (1-D)	• Two dimensions in the nanoscale but one dimension lies outside of the scale. • Examples: nanotubes and nanorods.

Table 1.1: continued.

Two-dimensional (2-D)	• Only one dimension lies in the nanoscale, the remaining two dimensions are outside of the scale. • Examples: nanolayers and nanofilms.
Three-dimensional (3-D)	• All dimensions are not confined to nanoscale. • Nanowire and nanotube arrays

1.2.1 Applications of nanoparticles

Nanoparticles have wide range of applications in various field due to its unique properties. It can be utilized in the healthcare industries, electronics equipment, agricultural industries, food industries, construction industries and cosmetics industries. The applications of nanoparticles are tabulated in Table 1.2.

Table 1.2: Applications of nanoparticles in various fields (Malik, Muhammad and Waheed, 2023).

Type of industry	Application
Medicine	• Used for cancer diagnosis and photothermal therapy of cancer. • Gadolinium nanoparticles used for inhibiting the growth of tumour. • Drug delivery to targeted cells (Joudeh and Linke, 2022).
Food	• Used in food manufacturing and packaging. • Nanoparticles help to improve processing method and extend shelf life of food products. • Nanoparticles act as antimicrobial agent to inhibit the growth of microbial in stored food products.
Agricultural	• Used for production, packaging, storing and transporting agricultural products. • Nanoparticles enhance the absorption of plant nutrients and provide better pathogenic detection against agricultural diseases.
Construction	• Nanoparticles serve as binding agent in cement to improve its strength and durability. • Involved in repairing mortars and concrete that help in crack recovering in buildings.

Table 1.2: continued.

Cosmetic	• Titanium dioxide (TiO_2) and zinc oxide (ZnO) are the main ingredient in making sunscreen (Dreno et al., 2019).

1.2.2 Synthesis method of nanoparticles

There are three methods to synthesize nanoparticles which are physical, chemical, and biological method as shown in Figure 1.1. In physical and chemical method, they involve in top-down approach which is first starting with the bulk materials and break down into smaller particles within the nano-size range (Weldegebrieal, 2020). The production of nanoparticles through these conventional physical and chemical methods are less favourable to be utilized in recent years. This is because these methods lead to the production of toxic and hazardous byproducts that are not environmentally friendly. In addition, the nanoparticles produced by these methods are not suitable for medical application due to health concerns, particularly in the clinical fields. Large amount of nanoparticles with precise size and shape can be produced in shorter time by these conventional techniques. However, these methods are sophisticated, expensive, and outdated. Thus, the biological method was introduced as it does not produce harmful waster during the synthesis process (Patra and Baek, 2014). Biological method utilizes bottom-up approach. It involves the nucleation of the atom, molecules or the ions in the solution followed by aggregation to form nano-size particles. This method was introduced due to its simplicity and more convenient as compared to top-down approach. Hence, biological method is

more widely used method to produce nanomaterials in the industry as it is a green method (Roy et al., 2021). Biological method uses microorganisms or plant extracts along with the precursor salt to form desired nanoparticles as shown in Figure 1.2. The biological method is more advantageous as it is cost effective, environmentally friendly and produce high purity product with simpler procedure (Weldegebrieal, 2020).

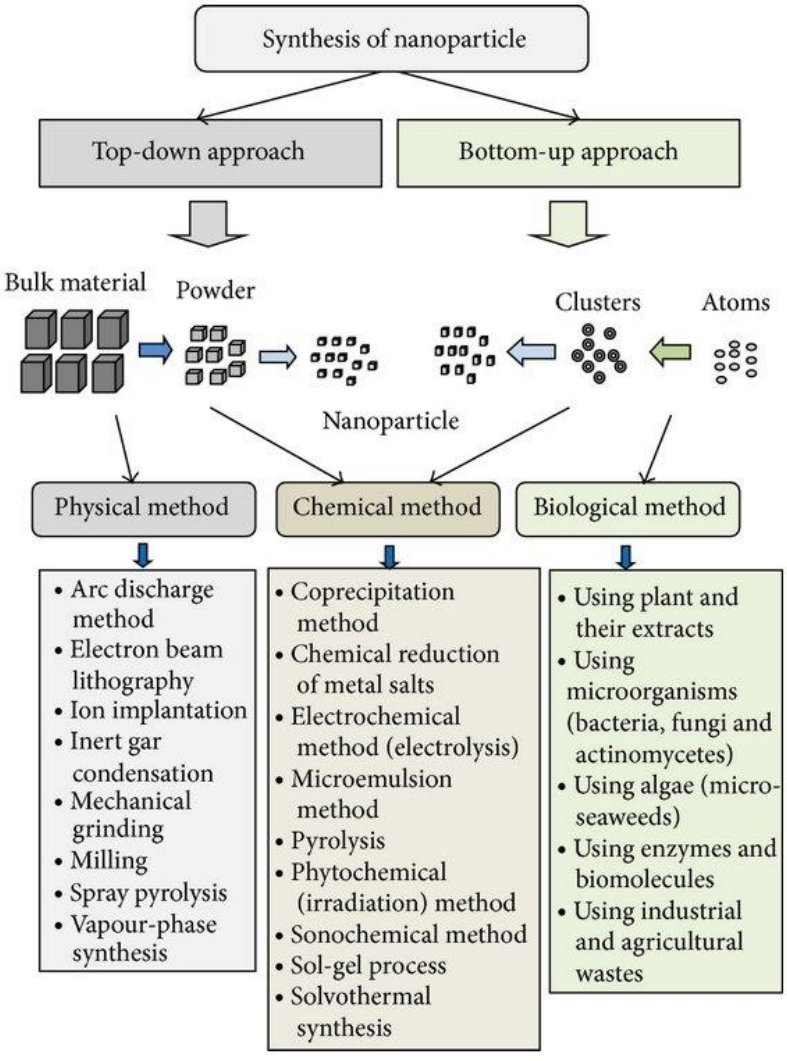

Figure 1.1: Synthesis of nanoparticles using top-down and bottom-up approach (Patra and Baek, 2014).

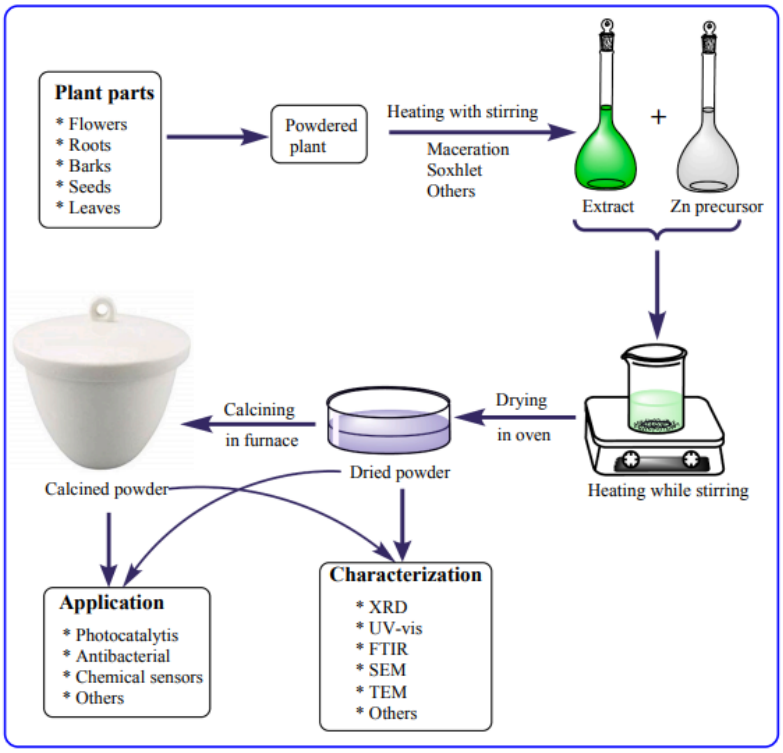

Figure 1.2: Biosynthesis of nanoparticle using plant extracts (Weldegebrieal, 2020).

1.3 Zinc oxide nanoparticle (ZnO NPs)

Zinc oxide nanoparticles have attracted significant research attention due to their potential application in various fields. It is the second most abundant metal oxide which is cost effective, safe, and can be readily available (Lakshmipriya and Gopinath, 2021). ZnO exists in white powder, and it is insoluble in water (Ahmaruzzaman and Raha, 2022). There are several possible polymorphs of ZnO such as hexagonal wurtzite, rock salt and zinc blende (Sponza, Jacek Goniakowski and Noguera, 2015). Both rock salt and zinc blende are not stable under room temperature. High pressure is required to synthesized rock salt

whereas zinc blende can be stabilized only on cubic substrates. At room temperature, wurtzite phase is the most thermodynamically stable. It exhibits tetrahedral geometry with each zinc atom is bonded to four oxygen atom tetrahedrally. In rock salt phase, each zinc atom has six neighbours while wurtzite and zinc blende has only four neighbours. Tetrahedral geometry is observed in both wurtzite and zinc blende. The main difference between them is the angle between the adjacent tetrahedral units, zero in wurtzite and 60° in zinc blende. Furthermore, the bond ionicity of wurtzite and zinc blende is also different. Wurtzite has a bond ionicity that lies between ionic and covalent which causes it to be thermodynamically stable while covalent character is found in zinc blende (Weldegebrieal, 2020). The different polymorphs of ZnO NPs are illustrated in Figure 1.3. However, the diverse synthesis methods and different materials used will alter the ZnO morphology which will affect the physical and chemical properties to be altered (Ahmaruzzaman and Raha, 2022).

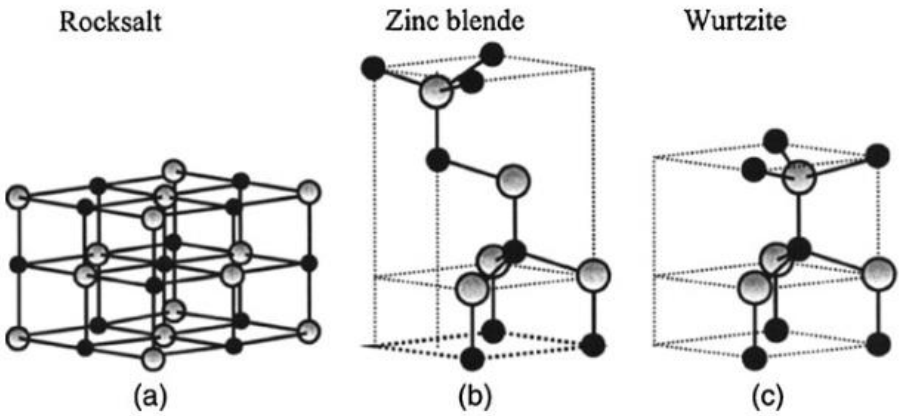

Figure 1.3: Crystal structures of ZnO NPs (Espitia et al., 2012).

ZnO is extensively used in various applications due to its unique characteristics credited to the unique optical, magnetic, electrical, morphological, catalytic, mechanical and photochemical properties (Pushpalatha et al., 2022). ZnO NPs are utilized in different field as it possesses excellent antibacterial activity even at low concentration. They can demonstrate potency against a wide range of bacteria (Selvanathan et al., 2022). Therefore, ZnO NPs are capable to act as antimicrobial agent (Sirelkhatim et al., 2015), photocatalyst to be used in photodegradation (Ong, Ng and Mohammad, 2018)

1.4 Green chemistry

Recently, there are more researchers utilize the combination of nanotechnology and the principles of green chemistry to create a sustainable environment in 21st century (Virkutyte and Varma, 2011). There are 12 principles in the green chemistry proposed by Paul Anastas and John Warner in 1998. The list of 12 principles of green chemistry is shown in Figure 1.4. The main concept of green chemistry is to leverage the chemical skills and knowledge to reduce the use of toxic chemicals and prevent the harmful waste produced which might contribute to environmental and health issues (Marco et al., 2019). The green synthesis of ZnO NPs from plant extract fulfilled the principles of green chemistry.

Figure 1.4: List of 12 principles of green chemistry (Juliana, 2022).

1.5 Malayan Cherry (*Muntingia calabura*)

In this study, the bark extracts of *Muntingia calabura* will be used to synthesize ZnO NPs. *Muntingia calabura* which is more commonly known as Malayan Cherry. It belongs to the Muntingiaceae family which can be found in Southeast Asia countries such as India, Indonesia, Philippines and Malaysia (Ansori, Kharisma and Solikhah, 2021). It is more commonly to be found at the side of the road. The height of the tree is about 3 - 12 meters, and the shape of the leaves is ovate-lanceolate that have a smooth feathered surface appears in dark green colour (Flora & Fauna Web, 2021). The flowers of *Muntingia calabura* have white petals with yellow stamens and are slightly small. The colour of the fruit

initially appears as green, but it turns to red when it ripens. Figure 1.4 illustrates different parts of the plant including the leaves, fruits and flower.

(a) Leaves (b) Fruits (c) Flower

Figure 1.5: Different part of *Muntingia calabura* (a) Leaves; (b) Fruits; (c) Flowers.

Various parts of the *M. calabura* such as the leaves, fruits, barks, stems and the leaves have different medicinal properties due to the presences of phytochemicals in the plant. The properties include antihypertensive, antidiabetic, antiseptic, antioxidant, and anti-inflammatory as well as protection against cough, flu, fever and headache (Ansori, Kharisma and Solikhah, 2021). However, the medicinal properties vary in different countries. In Peru, the bark and flowers are used as an antiseptic to reduce the swelling in lower extremities (Mahmood et al., 2014). Moreover, boiling the leaves in water can help to treat gastric ulcer and reduce prostate gland swelling (Zakaria et al., 2007). In Colombia, the infusion of the flower served as a tranquilizer and tonic. *M. calabura* has the ability to treat measles, mouth pimples and stomach-ache in

Mexico (Yasunaka et al., 2005). Other than the medicinal applications, the fruits can be made into jam to be used in food and beverage.

1.6 Objectives

This research aims to synthesize and characterize zinc oxide nanoparticles from plant extract. The specific objectives are listed below:

1. To synthesize zinc oxide nanoparticles (ZnO NPs) through green synthesis pathway using aqueous extract of bark of Malayan Cherry (*Muntingia calabura*).

2. To characterize zinc oxide nanoparticles (ZnO NPs) using Fourier Transform Infrared Spectroscopy (FTIR), UV-Visible Spectroscopy (UV-Vis), X-ray Diffraction (XRD), Field Emission Scanning Electron Microscopy (FESEM) and Energy Dispersive X-ray Spectroscopy (EDX).

CHAPTER 2

LITERATURE REVIEW

2.1 Green synthesis of zinc oxide nanoparticles

Nowadays, there is an increasing number of researchers that are interested in synthesizing nanoparticles through green synthesis pathway as compared to the conventional physical and chemical methods. This is because the conventional methods yield issues related to environment and the complexity of the reaction condition (Ying et al., 2022). The green synthesis of nanoparticles adheres to the 12 principles of green chemistry proposed by Paul Anastas and John Warner in 1998. The principles promote the use of renewable and green energy sources, reducing the harmful byproducts and waste generated. Safer chemicals, solvents and mild conditions are carried during the reaction (Anastas and Warner, 1998). Hence, this green synthesis is advantageous and will be safer than those conventional methods.

This research utilized the principles of green chemistry to ZnO NPs. The barks of *Muntingia calabura* was used as the green and renewable sources to synthesize ZnO NPs. In addition, the reaction does not involve the use of harmful and hazardous chemicals which will eliminate the toxic waste generated. The only solvent used will be the ionized water which is environmentally friendly. The phytochemicals that found in the plant act as the reducing agent and stabilizer to reduce the zinc ions, Zn^{2+} to Zn^{0}. There are large amounts of

phytochemicals found in the plant extract such as polyphenols, flavonoids, alkaloids and saponins which are the secondary metabolites that are important for the formation of stable nanoparticles (Selvanathan et al., 2022).

According to the research conducted by Selvanathan et al (2022), ZnO NPs were synthesised through the biosynthesis method where the phytochemicals found in the *Annona muricata* leaf extract act as the reducing and stabilizing agent that are responsible for the reduction process.

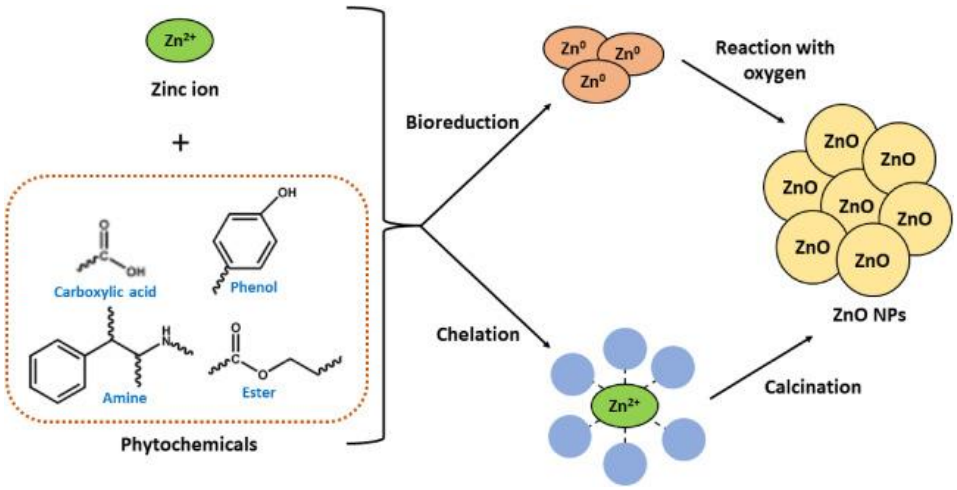

Figure 2.1: Proposed mechanism to synthesize ZnO NPs using *Annona muricata* leaf extract (Selvanathan et al., 2022).

2.2 Phytochemicals compositions in *Muntingia calabura.*

Plant extracts often served as the primary source of remedies in the field of traditional medicine for treating various diseases. Extraction from different parts of the plant such as the leaves, stems, barks, roots, flower and fruits possessed

potential therapeutic properties due to the presence of wide range of phytochemicals. For instance, alkaloids, flavonoids, tannins, saponins and phenols. In western countries, traditional medicine is often used in conjunction with modern medicine. In worldwide, there are over 80% of the population is replying on traditional medicine as the primary healthcare needs (Priya and Yasmin, 2022). The presence of these secondary metabolites allows the *Muntingia calabura* to possess antimicrobial, antioxidant and cytotoxic activity. Therefore, phytochemicals screening in *M. calabura* is important to determine the secondary metabolites that present in the plant. There are several chemical tests could be performed to confirm the presence of phytochemicals. On top of that, the FTIR could be carried out to further identify the functional groups of these phytochemicals to prove their existence. Table 2.1 listed the types of phytochemicals that present in the plant.

Table 2.1: Phytochemicals screening of *Muntingia calabura* extract (Priya and Yasmin, 2022).

Phytochemicals	Test/Reagent used	Observation	Aqueous extract
Alkaloids	Wagner's test	Formation of reddish-brown precipitate.	+
Flavonoids	Mg powder + HCl	Solution turned red.	+
Tannins	Ferric chloride test	Solution turned greenish black	+

Table 2.1: continued.

Saponins	Foaming test	Formation of foam when extract is shaken with water.	+
Phenols	Potassium dichromate	Formation of brown precipitate.	+
(+): Indicates presence ; (-): indicates absence			

2.3 Green synthesis of ZnO NPs using plant extract.

The application of nanotechnology in the biosynthesis of metallic nanoparticles utilized various plant resources is known as phytonanotechnology which is emerging as a promising new field of research. The harmful chemicals and complex reaction conditions are avoided in this technique. The presence of the functional components such as the phytochemicals that found in the plant make the plant extract significantly more advantageous. Phytochemicals possess medicinal activity, and they are classified into two classes which are primary metabolites and secondary metabolites. The primary metabolites include carbohydrates, proteins, amino acids, chlorophylls, and lipids. Other phytochemicals such as flavonoids, alkaloids, phenolics, tannins and saponins are classified as secondary metabolites (Bhardwaj et al., 2019). The different parts of the plants such as the stems, barks, leaves and roots act as the capping and reducing agents for the plant-mediated synthesis of metallic nanoparticles. This synthesis method is environmentally friendly as it utilizes the plant resources and milder reaction condition which is suitable for synthesizing the nanoparticles in large quantities (Mathew, 2020).

In this literature review, green method was utilized to synthesis ZnO NPs from bark extracts (*Cinnamomum verum* and *Amygdalus scoparia*) leaves extract (*Annona muricataI* L. and *Aloe barbadensis miller*) and lastly fruits extract (*Rubus ellipticus and Myristica fragrans*).

2.3.1 Green synthesis and characterization of ZnO NPs using bark extract of Cinnamon (*Cinnamomum verum*)

Research on the synthesis of ZnO NPs using *Cinnamomum verum* bark was done by Shanmugam et al (2022) to prevent the growth of KB cancer cell and trigger apoptosis in KB cancer cell. *Cinnamomum verum* is more commonly known as cinnamon (Flora & Fauna Web, 2020). It was found that the bark extract of *C. verum* consist of bioactive ingredients that can be used to treat disease due to its pharmacological actions such as antibacterial, antifungal and antibiofilm. The synthesized ZnO NPs derived from *C. verum* possessed anticancer activity against oral cancer. The bark extract of *C. verum* act as the reducing and stabilizing agent and the precursor used is zinc nitrate hexahydrate. The overall procedure of the green synthesis is shown in Figure 2.2.

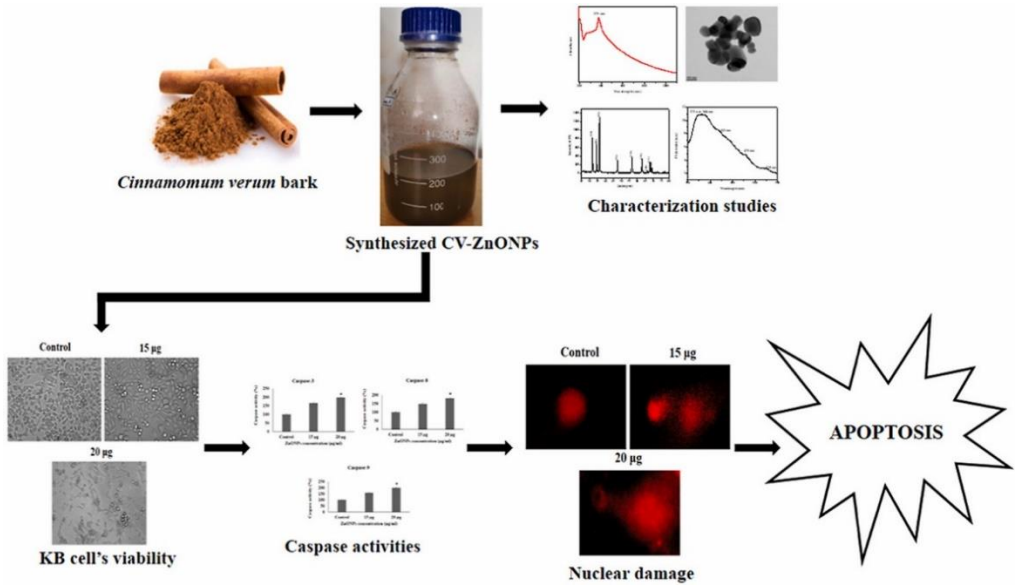

Figure 2.2: Schematic illustration of green synthesis of ZnO NPs derived from *C. verum* bark extract (Shanmugam et al., 2022).

The synthesized ZnO NPs was confirmed by several characterization. Based on the TEM analysis as shown in Figure 2.3(a), the synthesized ZnO NPs are uniformly distributed with a spherical shape and an average size ranging from 30 to 45 nm. The elemental composition was determined by EDX as shown in Figure 2.3(b). The EDX spectrum reveals that both zinc and oxygen are present with no impurities found. This indicates that the synthesized ZnO NPs have high purity.

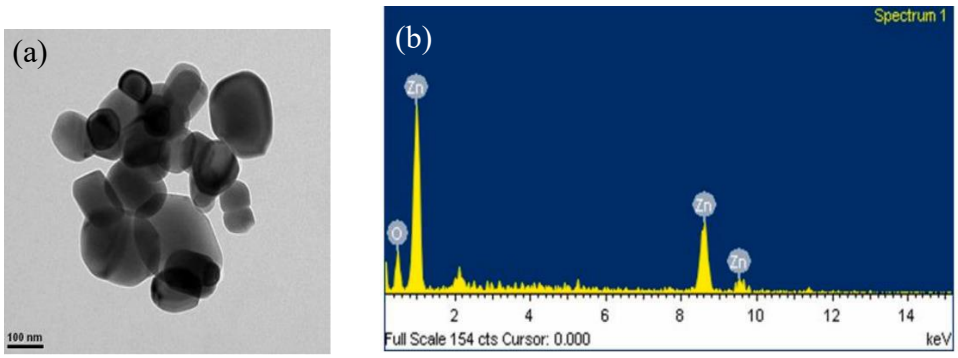

Figure 2.3: (a) TEM image, (b) EDX analysis of ZnO NPs (Shanmugam et al., 2022).

Based on the UV-Vis spectrum as shown in Figure 2.4(a), the maximum absorption peak at 379 nm indicates the formation of ZnO NPs. Figure 2.4(b) shows the FTIR spectrum of ZnO NPs. The peaks at 3421 cm^{-1} correspond to the presence of O-H stretching. The C-H stretching can be observed at 2985, 2934 and 2863 cm^{-1}. The peaks at 1582 and 1429 cm^{-1} represent the C=C stretching while C=O stretching is indicated at 1121 and 1012 cm^{-1}. The peaks at 435 cm^{-1} revealed the presence of Zn-O stretching. The crystallinity of ZnO NPs was determined by XRD which is shown in Figure 2.4(c). The diffraction peak observed at (100), (002), (101), (102), (110), (103), (200), (112), and (201) planes as evidence of crystalline nature of ZnO NPs with an average size of 35.69 nm. There are no other unrelated peaks in the XRD spectrum which indicates that the synthesized ZnO NPs are pure.

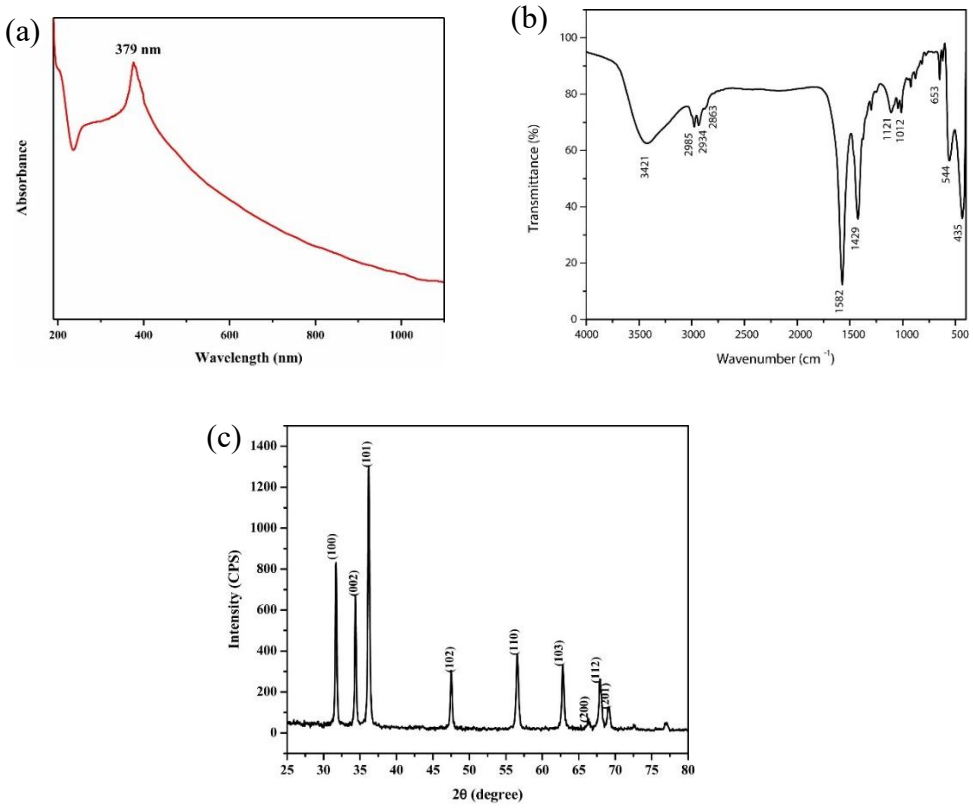

Figure 2.4: (a) UV-Vis spectrum, (b) FTIR spectrum, (c) XRD pattern of ZnO NPs (Shanmugam et al., 2022).

2.3.2 Green synthesis and characterization of ZnO NPs using bark extract of *Amygdalus scoparia.*

Jobie, Ranjbar and Moghaddam (2021), conducted a study on synthesis of ZnO NPs using *A. scoparia* bark extract. *Amygdalus scoparia* belongs to the Rosacea family that is native to Iran region. In Iran, this species is widely used to treat diseases that are related to cardiovascular, respiratory, diabetes, cancer, diarrhea and the list goes on. In this study, the bark extract of *A. scoparia* is found to possess antidiabetic and anticancer activity. In the synthesis of ZnO NPs derived from the plant, the bark extract was responsible as the reducing agent and the salt precursor used was zinc acetate dehydrates. The formation of ZnO NPs was further confirmed by several characterization such as TEM, EDX, XRD, UV-Vis and FTIR.

Figure 2.5: *Amygdalus scoparia* tree (Govaerts et al., 2021).

Based on Figure 2.6(a), the FESEM image reveals that the ZnO NPs exhibited spherical shape, ranging between 15 and 40 nm with an average size of 29 nm. The TEM analysis as shown in Figure 2.6(b) indicates that the size range of the

synthesized spherical ZnO NPs was 10 to 60 nm. The elemental composition of the ZnO NPs could be further confirmed by EDX analysis. Based on Figure 2.6 (c), it could be observed that there was total of three peaks where two peaks belong to the zinc and the remaining one peak indicated the presence of oxygen with a weight percent of 68.7% and 31.3% respectively. This confirmed that the formation of ZnO NPs was pure.

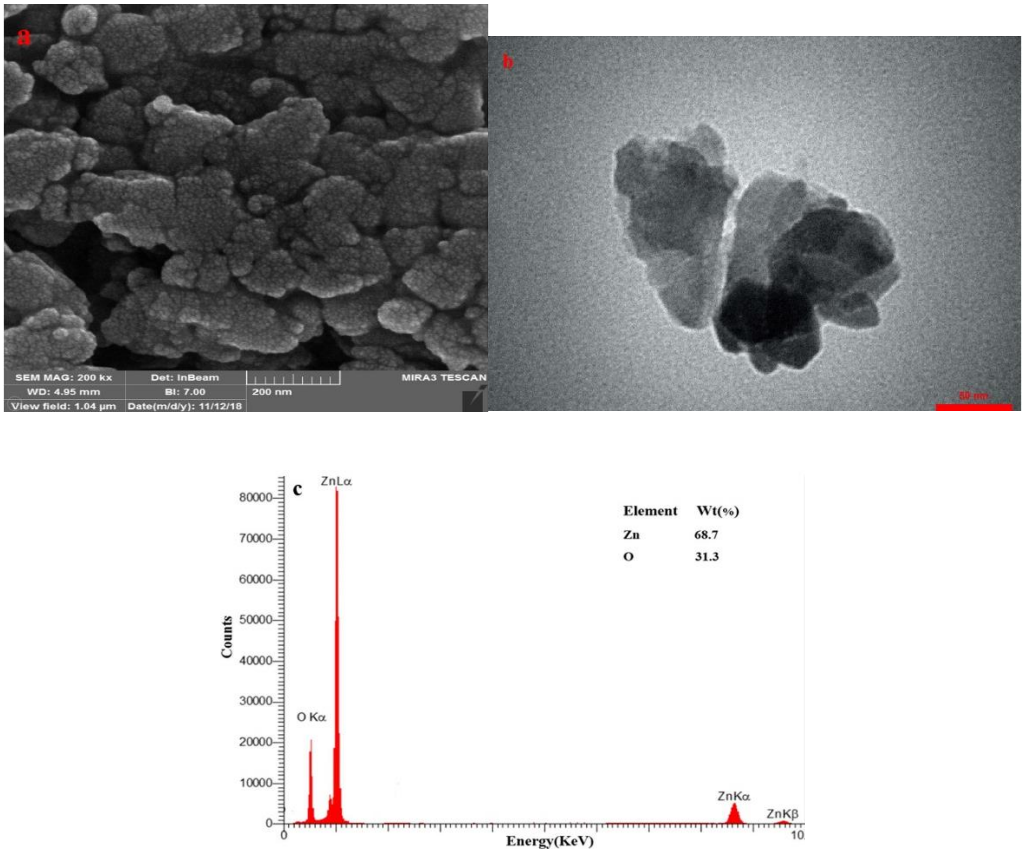

Figure 2.6: (a) FESEM image, (b) TEM image, (c) EDX analysis of ZnO NPs (Govaerts et al., 2021).

The formation of ZnO NPs could be further confirmed by the presence of the ZnO NPs functional group in the FTIR spectrum as shown in Figure 2.7. It could be observed that there was a shifting of the absorption band due to the interaction of the ZnO NPs with the phytochemicals in the plant extract. The broad peaks

located at 3429.9 cm^{-1} was due to the N-H band of the protein and O-H band of phenol and alcohol. The symmetric and asymmetric stretching of the band located at 2924.9 cm^{-1} and 1723.2 cm^{-1} corresponded to the CH_2 stretching of the lipid or carbohydrates and C=O band in the carboxyl or C=C stretching in the aromatic ring respectively. The peaks at 1405 cm^{-1} represented the COO- in the amino acid and stretching of CH_3 of fatty acid. The presence of C-O stretching in carbohydrate could be observed at 1265.8 cm^{1} and the peak at 1082.9 cm^{-1} was due to the C-O stretching of oligosaccharide residue. Lasty, the formation of ZnO NPs could be observed at 481.3 cm^{-1}.

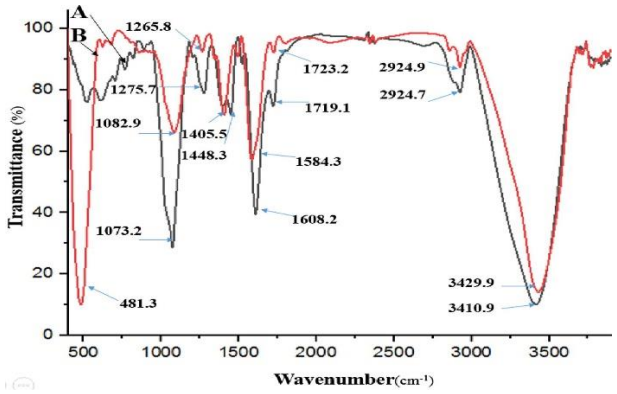

Figure 2.7: FTIR spectrum of (a) *A. scoparia* extract (b) synthesized ZnO NPs (Govaerts et al., 2021).

In Figure 2.8(a), the maximum absorption peak at 368 nm indicated the formation of ZnO NPs. The crystallinity and average crystallite size of ZnO NPs were determined by XRD analysis as shown in Figure 2.8(b). The presence of sharp peaks in the XRD diffractogram at 2θ of 31.9°, 34.6°, 36.45°, 47.75°, 56.8°, 62.9°, 65.8°, 68.15°, 68.9°, 72.7°, and 77.2° were corresponded to (100), (002), (101), (102), (110), (103), (200), (112), (201), (004) and (201) crystal

planes that indicated a hexagonal structure with an average crystallite size of 19.14 nm calculated by Debye Scherer's equation.

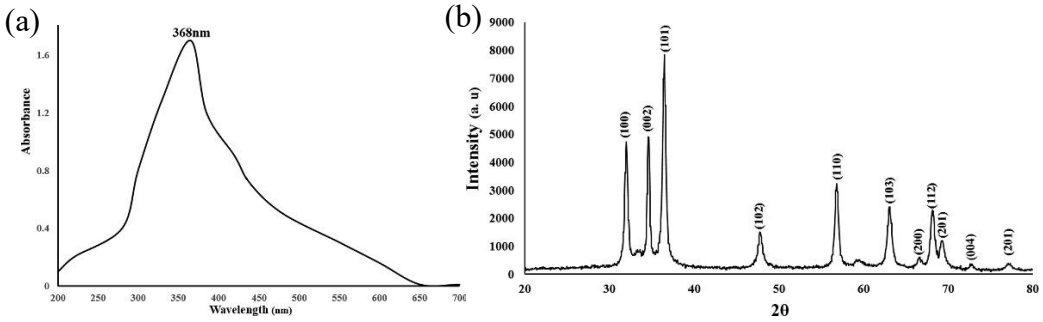

Figure 2.8: (a) UV-Vis spectrum, (b) XRD pattern of ZnO NPs (Govaerts et al., 2021).

2.3.3 Green synthesis and characterization of ZnO NPs using soursop (*Annona muricata* L.) leaf extract.

In this work reported by Selvanathan and his co-worker (2022), ZnO NPs were synthesized using the soursop (*Annona muricata*) leaf extract. *Annona muricata* belongs to the Annonaceae family that has been widely used in the field of traditional medicine to treat many diseases (Mutakin et al., 2022). The green reducing agent used was *A. muricata* leaf extract along with the zinc nitrate hexahydrate as the precursor salt for the formation of ZnO NPs. Deionized water served as the green solvent as it is non-toxic and safer to be used.

Figure 2.9: *Annona muricata* L. (Bionutricia, 2023).

In this research, microwave irradiation technique was used rather than the conventional heating method. The conventional heating method depends on the heat transfer through conduction and convection which is less efficient. On the contrary, the microwave irradiation promotes effective heating and material penetration. This allows the reaction to be completed in shorter time with high purify and yield of products. The microwave irradiation was used at 250 W at 80 ℃ for about 15 minutes for the radiation until a formation of reddish-brown solution. The white ZnO NPs obtained was further characterized. The green synthesis procedure is shown in Figure 2.10.

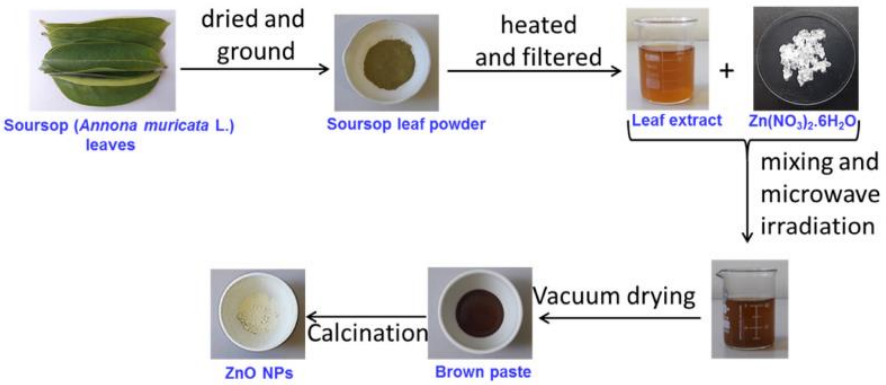

Figure 2.10: Procedure for green synthesis of ZnO NPs utilizing *Annona muricata* leaf extract (Selvanathan et al., 2022).

Based on the SEM image as shown in Figure 2.11(a), the morphology of ZnO NPs are quasi-spherical nanostructures that is uniformly distributed. The elemental composition of the synthesized ZnO NPs was identified to consist of only zinc and oxygen, indicating the ZnO NPS produced are high purity (Figure 2.11(b)).

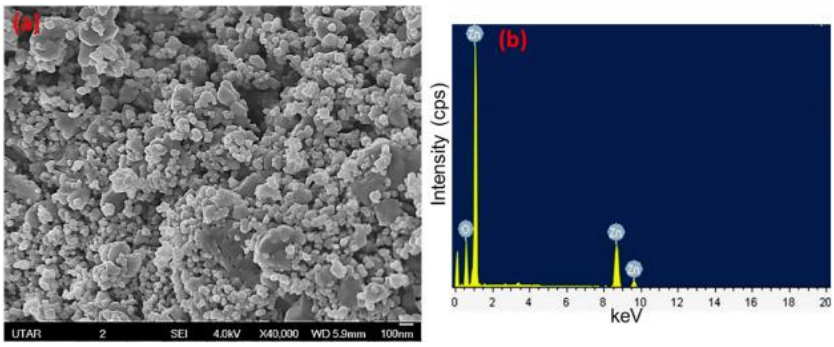

Figure 2.11: (a) FESEM images of ZnO NPs at 40000× magnification, (b) EDX spectrum of ZnO NPs (Selvanathan et al., 2022).

Based on the TEM analysis, the size of ZnO NPs is ranging from 20 nm to 50 nm. The average particle size is found to be 37 nm based on the particle size distribution histogram.

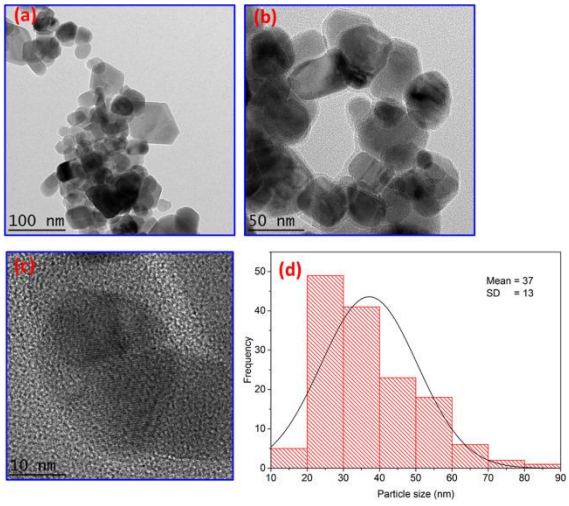

Figure 2.12: (a to c) TEM images, (d) Particle size distribution histogram of ZnO NPs (Selvanathan et al., 2022).

The FTIR spectrum of *A. muricata* leaf extract as shown in Figure 2.13(a) is to determine the presence of secondary metabolites. The presence of O-H bond of the polyphenols and C-O stretching of flavonoids are indicated by the peak located at 3550 cm^{-1} and 1740 cm^{-1} respectively. The broad absorption between 1400 and 1600 cm^{-1} refers to the C-N bond from the alkaloids. In Figure 2.13(b), the formation of ZnO NPs could be observed at 466 cm^{-1} absorption band. Some of the phytochemicals are detected in the FITR spectrum of the synthesized ZnO NPs. The shifting of peaks indicates that phytochemicals chelate with zinc ions forming metal-coordinated complexes or the Zn^{2+} ion undergo bio-reduction by the phytochemicals. The proposed mechanism is illustrated in Figure 2.1.

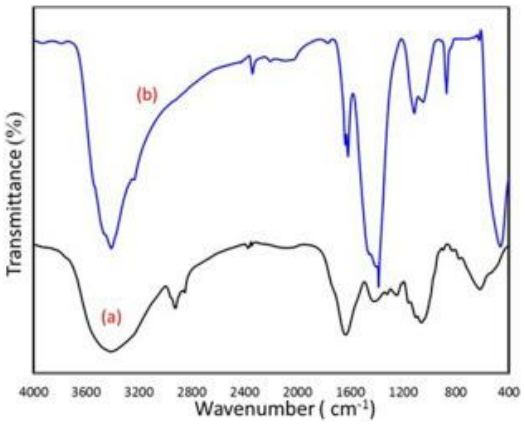

Figure 2.13: FTIR spectrum of (a) *A. muricata* leaf extract, (b) ZnO NPs obtained (Selvanathan et al., 2022).

Figure 2.14(a) shows the XRD spectrum of ZnO NPs. The sharp and intense peak indicates the crystalline ZnO NPs with a hexagonal wurtzite structure that have a crystallite size ranges between 10 and 20 nm. Figure 2.14(b), the

maximum absorption peak of ZnO NPs at 365 nm with a band gap energy of 3.39 eV.

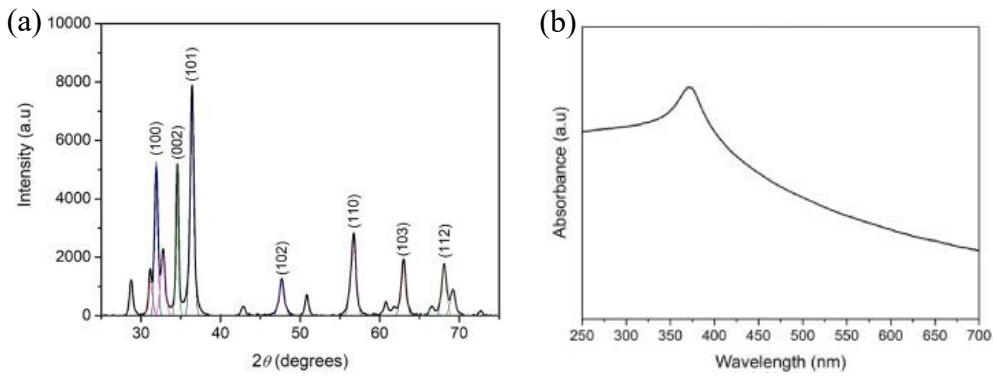

Figure 2.14: (a) XRD spectrum, (b) UV-Vis absorption spectrum of ZnO NPs (Selvanathan et al., 2022).

2.3.4 Green synthesis and characterization of ZnO NPs using aloe vera (*Aloe barbadensis miller*) leaf extract.

Aloe barbadensis miller which is more commonly known as aloe vera belongs to Asphodelaceae family. Aloe vera is widely utilized until today's century due to its medicinal attributes in the field of healthcare and dermatology (Surjushe, Vasani and Saple, 2008). In this research conducted by Singh and his co-worker (2019), the formation of ZnO NPs were synthesized through both chemical and green synthesis method to study the differences in the properties such as particle size. The different route of synthesis method was illustrated in Figure 2.15. In chemical synthesis, the ZnO NPs were formed by reacting the zinc acetate precursor with the sucrose solution followed by the addition of NaOH solution through the sol-gel technique. In the green synthesis method, the aloe vera extract acted as the reducing and stabilizing agent to react with zinc acetate. In

this case, the phytochemicals in the plant extract reduced the zinc acetate to the metallic zinc and calcinated at 400 ℃ to form ZnO NPs. The ZnO NPs obtained were subjected to characterization.

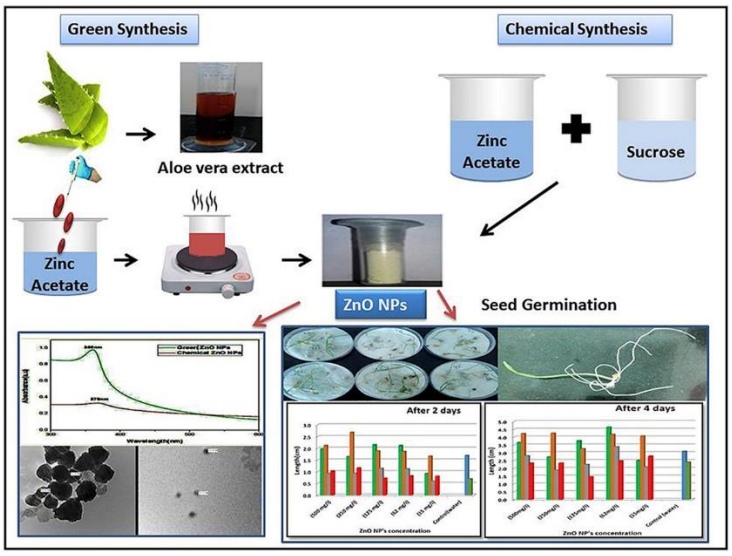

Figure 2.15: Green synthesis and chemical synthesis of ZnO NPs derived from aloe vera leaf extract (Singh et al., 2019).

Based on Figure 2.16(a) and (b), the SEM images of both synthesis method show that the ZnO NPs synthesized in the shape of spherical with aggregations. The chemical composition of chemically synthesized and green synthesized ZnO NPs was 50.39% of zinc, 19.99% of oxygen, 29.62% of carbon and 75.58% of zinc and 24.42% of oxygen respectively. This proves that the ZnO NPs synthesized through green method have a greater purity.

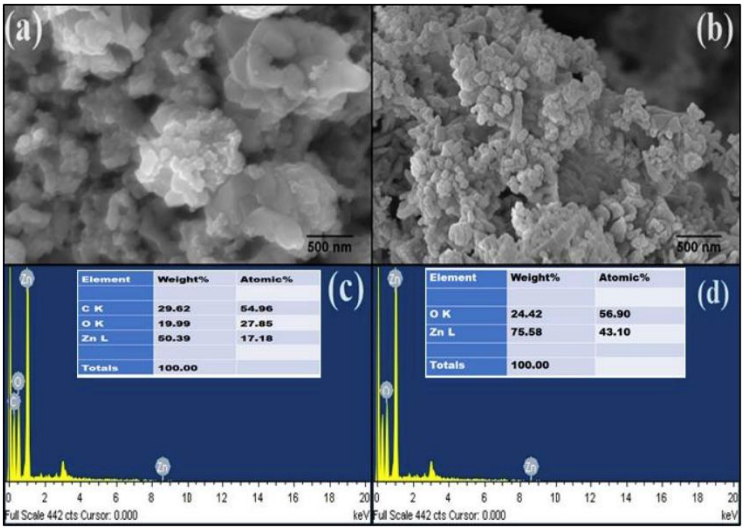

Figure 2.16: SEM images of (a) chemically synthesized ZnO NPs, (b) green synthesized ZnO NPs, and EDX spectrum of (c) chemically synthesized ZnO NPs, (d) greens synthesized ZnO NPs (Singh et al., 2019).

Figure 2.17(a) shows the chemically synthesized ZnO NPs were spherical shape with an average size of 42 to 56 nm. On the contrary, the green synthesized ZnO NPs as shown in Figure 2.17(b) were spherical and polycrystalline without aggregation with a smaller average size of 30 to 40 nm. It can be said that the particle size of green synthesized NPs is smaller than those chemically synthesized NPs due to the presence of phytochemicals in the plant extract that served as the stabilizing agent to prevent the aggregation of NPs to form more stable and smaller NPs.

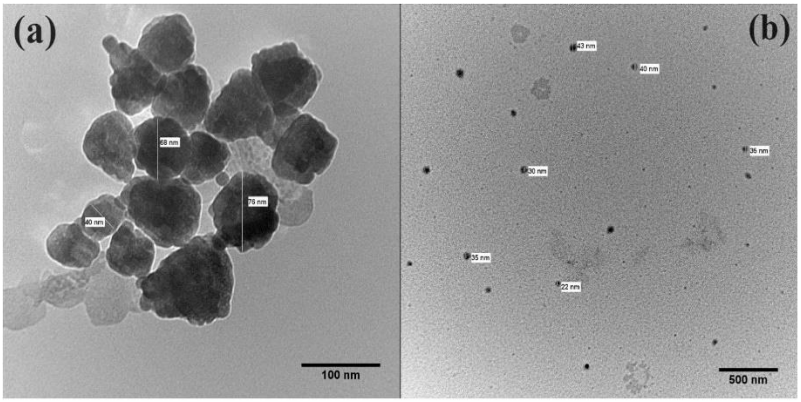

Figure 2.17: TEM images of (a) chemically synthesized ZnO NPs, (b) green synthesized ZnO NPs (Singh et al., 2019).

According to Figure 2.18, the green synthesized ZnO NPs had an absorption peak of 360 nm with a band gap energy of 3.44 eV, while the absorption peak of chemically synthesized ZnO NPs was 370 nm with a band gap energy of 3.35 eV. The difference in the absorption peak is due to the difference in the particle size. In the quantum confinement effect, the increased in the band gap energy causes the absorption peak shifts towards a lower wavelength resulted in smaller particle size. The green chemically synthesized ZnO NPs had a smaller size due to the reducing ability of the aloe vera extract.

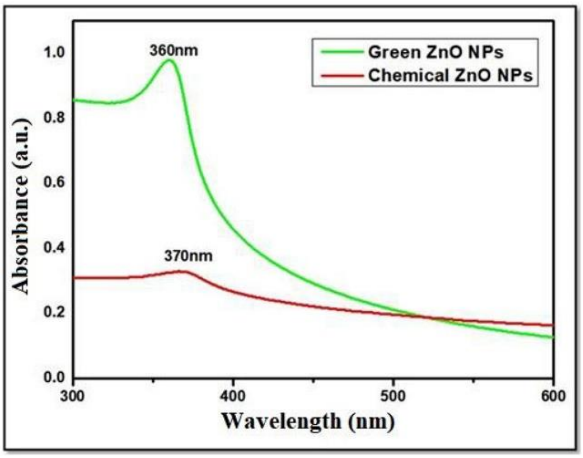

Figure 2.18: UV-Vis spectrum of chemically and green synthesized ZnO NPs (Singh et al., 2019).

The XRD pattern of both chemically and green synthesized ZnO NPs are shown in Figure 2.19(a) and (b) respectively. The diffraction peaks at 2θ were corresponded to hexagonal phase with a wurtzite structure. However, the average crystallite size of green synthesized and chemically synthesized of ZnO NPs were 32 nm and 45 nm respectively. The green synthesized ZnO NPs achieved a smaller crystallite size.

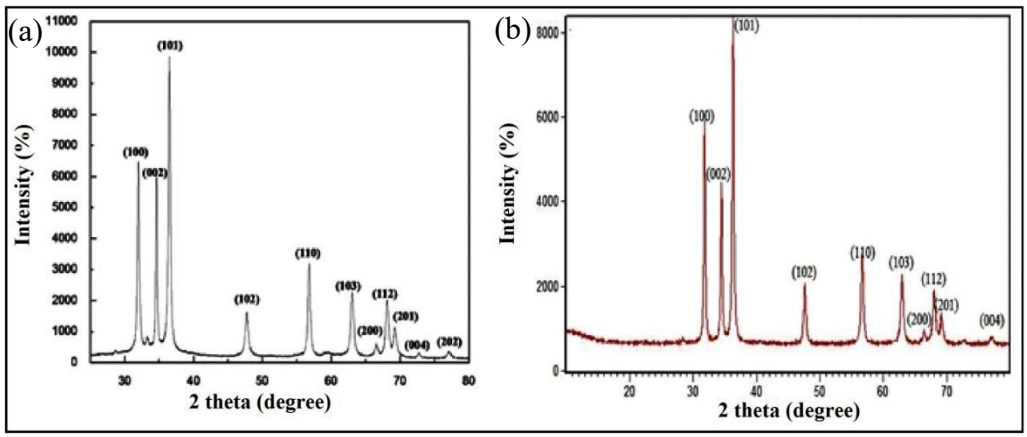

Figure 2.19: XRD analysis of (a) chemically and (b) green synthesized ZnO NPs (Singh et al., 2019).

2.3.5 Green synthesis and characterization of ZnO NPs using fruit extracts of Nutmeg (*Myristica fragrans)*.

In this work, Faisal et al. (2021) reported that ZnO NPs was synthesized using fruit extracts of *M. fragrans* as the reducing agent and stabilizing agent along with zinc nitrate as the precursor. *Myristica fragrans* belongs to Myristicaceae family and is native to the Maluku Island, Indonesia. This species is extensively utilized as an Indian traditional medicine to treat various illness due to its pharmacological properties (Ashokkumar et al., 2022). The experimental procedure is shown in Figure 2.20.

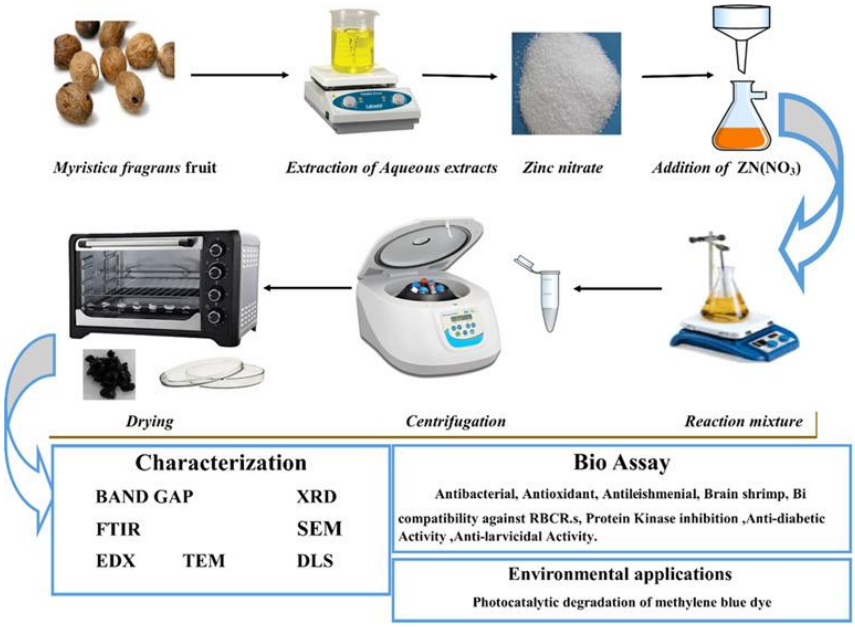

Figure 2.20: Experimental procedure of green synthesized ZnO NPs (Faisal et al., 2021).

Figure 2.21(A) and (B) reveal that the ZnO NPs synthesized have an agglomerated semi spherical to hexagonal shape. The ZnO NPs are in

homogenous dispersion with a particle size ranging from 43.3 - 83.1 nm. The EDX profile in Figure 2.21(C) identifies the presence of Zn and O with a weight percent of 65.30% and 21.00% respectively with traces of impurities present.

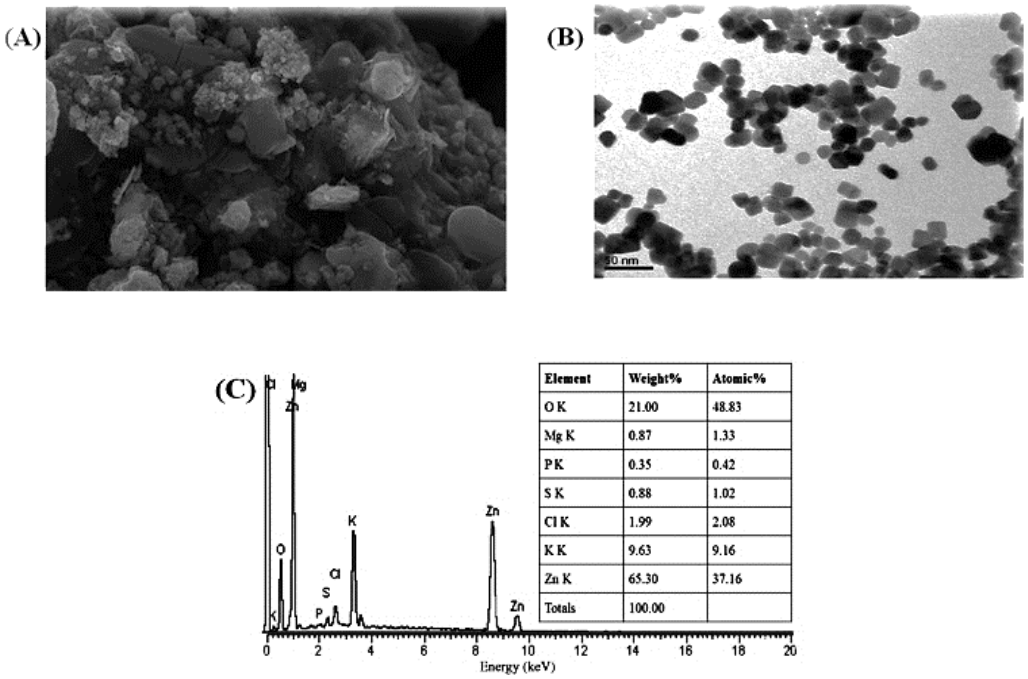

Element	Weight%	Atomic%
O K	21.00	48.83
Mg K	0.87	1.33
P K	0.35	0.42
S K	0.88	1.02
Cl K	1.99	2.08
K K	9.63	9.16
Zn K	65.30	37.16
Totals	100.00	

Figure 2.21: (A) SEM image, (B) TEM image, (C) EDX analysis of ZnO NPs (Faisal et al., 2021).

The synthesized ZnO NPs have a band gap energy of 2.57 eV (Figure 2.22(a)) which is considered as small band gap that has a great photocatalytic activity. It can be used as a photocatalyst for the dye degradation as the electrons can be excited easily from the valence band to the conduction band since the band gap is small. Figure 2.22(b) shows the FTIR spectrum of the ZnO NPs. The presence of ZnO is indicted by the peak located at 469 cm^{-1}. The weak absorption bands at around 3420 and 3200 cm^{-1} might be due to the O-H group stretching. There are some other peaks observed at around 1100, and 900 cm^{-1}. The peaks at 1100 cm^{-1} corresponding to the C-O stretching of carbohydrate and C=C rings. Both

primary and secondary metabolites are present in the plant extract. The 900 nm^{-1} absorption peak is due to the phosphodiester bond stretching. Based on the XRD analysis as shown in Figure 2.22 (c). the sharp and intense diffraction peaks at 31.5°, 34.4°, 36.2°, 47.5°, 56.4°, 62.8°, and 67.9° have been indexed as hexagonal wurtzite structure (JCPDF file no. 00-036-1451) with an average crystallite size of 41.23 nm.

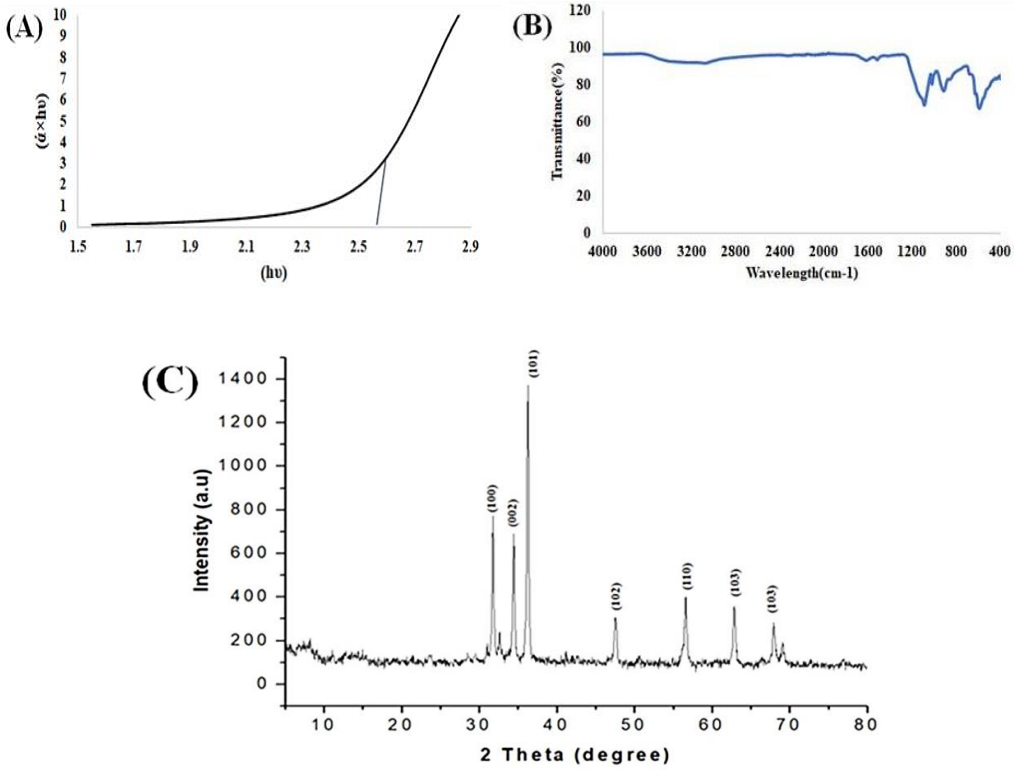

Figure 2.22: (A) Tauc's plot, (B) FTIR spectrum, (C) XRD diffractogram of ZnO NPs (Faisal et al., 2021).

2.3.6 Green synthesis and characterization of ZnO NPs using fruit extracts of yellow Himalayan raspberrry (*Rubus ellipticus)*.

The study on the green synthesis of ZnO NPs using *Rubus ellipticus* fruit extract was conducted by Dhatwalia et al. (2022). *Rubus ellipticus* has a common name of yellow Himalayan raspberry. It belongs to the Apocynaceae family which is native to Indonesia, China and Sri Lanka. The fruit extract was reported to possess anticancer, antioxidant and antimicrobial activity. The fruit extract acted as the reducing and stabilizing agent while the salt precursor used were zinc acetate dihydrate for the formation of ZnO NPs.

Figure 2.23: Yellow Himalayan rasberry (Flora of Sri Lanka, 2023).

Figure 2.24(a) shows SEM image of the synthesized ZnO NPs that had an agglomerated flower like structure. The TEM image as shown in Figure 2.24(b) reveals the formation of irregular shapes where the smaller grains diffused to form larger grains with an average particle size of 19.12 nm as represented by the particle size distribution in Figure 2.24(c).

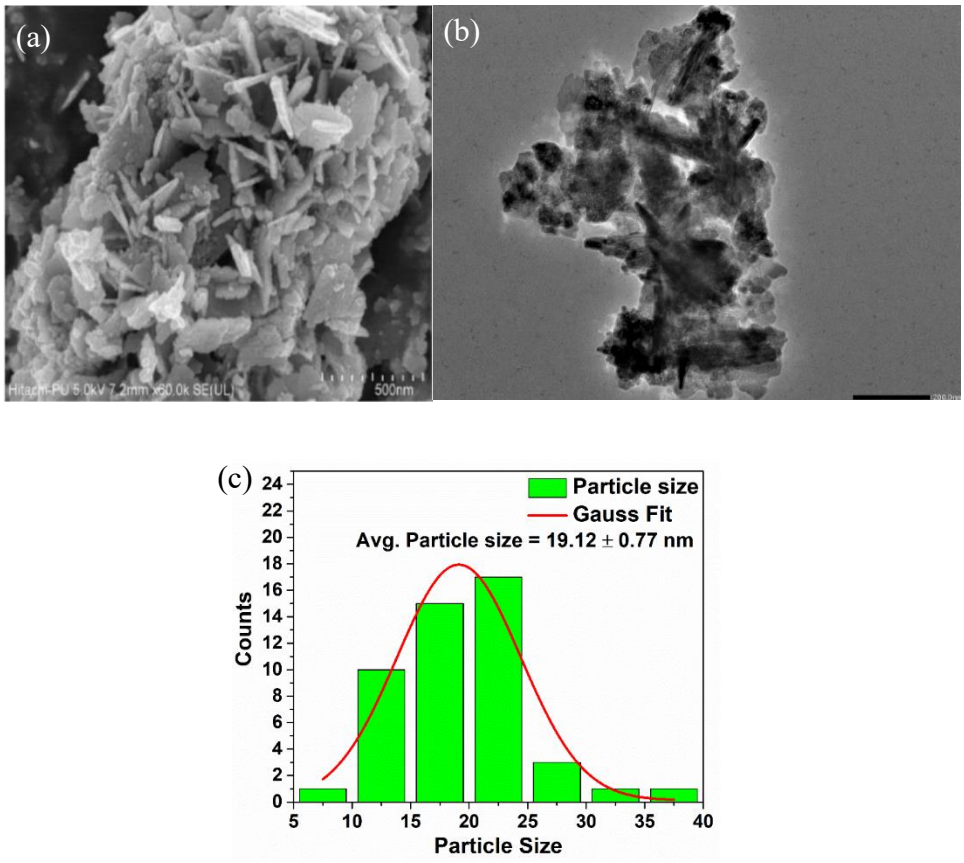

Figure 2.24: (a) SEM image, (b) TEM image, (c) Particle size distribution of ZnO NPs (Dhatwalia et al., 2022).

The synthesized ZnO NPs exhibits a maximum absorption peak at 353 nm (Figure 2.25(a)) with a band gap energy of 3.21 eV which was determined using Tauc's plot as show in Figure 2.25(b).

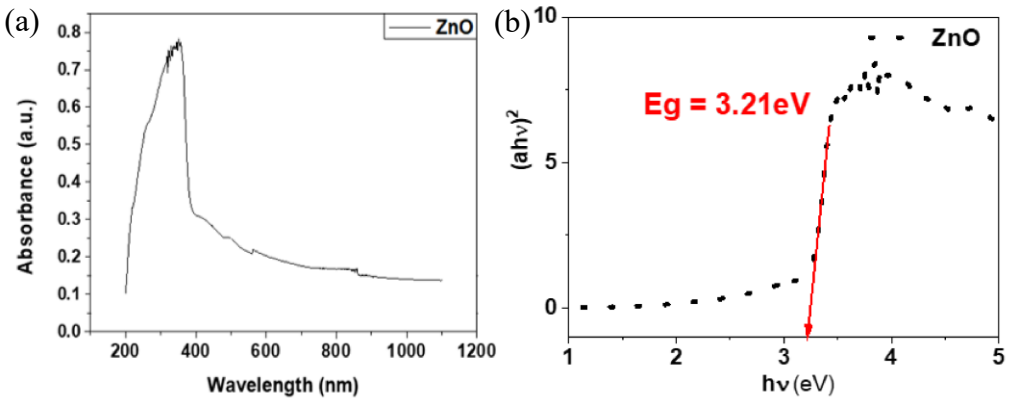

Figure 2.25: (a) UV-Vis spectrum, (b) Tauc's plot of ZnO NPs (Dhatwalia et al., 2022).

Based on Figure 2.26(a), the O-H group and the N-H stretching of carboxylic acids, alcohols and amide were located at 3432.9 cm^{-1} and 2926 cm^{-1}. However, the strong peaks around 3200 cm^{-1} to 3300 cm^{-1} were assigned to the overlapping of the N-H stretching with the O-H group in the fruit extract. The O-H group stretching was due to the presence of phenol and alcohol, while the N-H groups might be due to the presence of proteins. This proved that the presence of phytochemicals such as phenols, flavonoids, saponins and tannins in the fruit extract to act as the reducing agent. The peak located at 1626 cm^{-1} and 1395 cm^{-1} due to the C=C and C-N stretching of the aromatics and aromatic amines. The formation of ZnO NPs could be confirmed by the peak located at 563 cm^{-1}. The formation of ZnO NPs could be further determined by XRD analysis as shown in Figure 2.26(b). The diffraction peaks observed at 2θ were indexed as hexagonal wurtzite structure by matching well with the standard JCPDS card number 36-1451. The crystallite size of synthesized ZnO NPs was 20 nm by

using the Debye Scherer equation. The XRD analysis revealed that the absence of impurities.

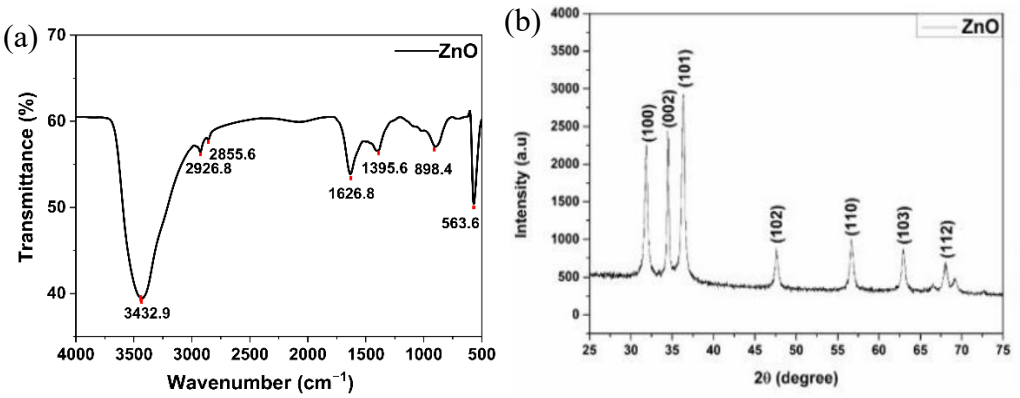

Figure 2.26: (a) FTIR spectrum, (b) XRD diffractogram of synthesized ZnO NPs (Dhatwalia et al., 2022).

2.4 Concluding remarks

Based on the previous studies, the green synthesis method was utilized to synthesize the ZnO NPs owning to its advantages over the conventional methods. The zinc nitrate hexahydrate was selected as the salt precursor and the reducing agent used in this study was the bark extract of *M. calabura*. This is because there is limited research studies and literature conducted on the green synthesis of ZnO NPs using bark extract. Therefore, the properties of the green synthesized ZnO NPs derived from the bark extract of *M. calabura* would be studied in this experiment. Table 2.2 provides a list of tables of the characterization of ZnO NPs synthesized from different sources and parts of plant. It can be proved that different parts of the plant are able to synthesize nanoparticles with the similar results.

Table 2.2: Research work using plant sources for the biosynthesis and characterization of ZnO NPs.

Plant [common name]	Precursor	Plant parts	Absorption peak (nm)	Wavenumber with predicted functional groups		Morphology	Particle size (nm)	Reference
Artemisia annua [Sweet sagewort]	Zinc nitrate	Barks	330	3012 2881 1697 535	O-H C-H C=C Zn-O	Spherical	33.1	(Wang et al., 2020)
Hylocereus polyrhizus [Dragon fruit]	Zinc nitrate	Peels	369	3432 1637 1248 460	O-H C=O C-O Zn-O	Spherical	56	(Aminuzzaman et al., 2019)

Table 2.2: continued.

Juglans regia [Walnut]	Zinc acetate	Leaves	355 – 370	3244, 3417 1624 439	O-H C=C Zn-O	Spherical	45 – 65	(Darvishi, Kahrizi and Arkan, 2019)
Ziziphus jujuba [jujube]	Zinc nitrate	Fruit	376	3420 1633 1049 640	O-H C=O C-O Zn-O	Spherical	29	(Golmohammadi, Honarmand and Ghanbari, 2020)

CHAPTER 3

MATERIALS AND METHODOLOGY

3.1 Materials

Barks of Malayan Cherry (*Muntingia calabura*) were collected from Block D, Universiti Tunku Abdul Rahman, Kampar, Perak, Malaysia. Zinc nitrate hexahydrate (molecular weight = 297.49 g/mol) with analytical research (AR) grade was purchased from Chemical Solutions Sdn Bhd and was kept in the drying cabinet as it is hygroscopic. It served as the precursor salt during the synthesis of ZnO NPs. Deionized water was used as the green solvent throughout the study.

3.2 Equipment

The equipment used throughout the study are listed in Table 3.2.1.

Table 3.2.1: List of equipment used and their function.

Equipment	Function
Analytical balance	To weight the mass of grinded plant powder, zinc nitrate hexahydrate and ZnO NPs.

Table 3.2.1: continued.

Centrifuge	To separate the supernatant and pellet of the bark extract.
Desiccator	To store the bark powder of *M. calabura* and zinc oxide nanoparticles for further usage.
Freeze dryer	To remove the moisture content in the bark extract of *M. calabura.*
Furnace	To perform calcination reaction at high temperature.
Grinder	To grind the dried barks of *M. calabura* into fine powder.
Hot plate with magnetic stirrer	To perform constant heating and stirring of plant extract.
Mortar and pestle	To grind the zinc oxide nanoparticle together with KBr when subjected to FTIR.
Oven	To dry the barks of *M. calabura*.
Sonicator	To disperse the zinc oxide nanoparticles in deionized water.
Thermometer	To monitor the temperature of the extract during heating.

3.3 Instrument

Table 3.3.1: List of instruments that used for the characterization of ZnO NPs.

Equipment	Model	Function
Fourier transform infrared spectrometer (FTIR)	PerkinElmer Spectrum RX 1	To determine the functional groups of bark extract and ZnO NPs.
UV-visible spectrophotometer (UV-Vis)	Thermo Fisher Scientific Genesys 180	To determine the maximum absorption peak and band gap energy.
Field emission scanning electron microscope (FESEM)	JEOL JSM-6701F	To identify the morphology and particle size of ZnO NPs.
Energy dispersive X-ray spectrometer (EDX)	Oxford Instruments X-Max 50mm^2	To determine the elemental composition of ZnO NPs.
X-ray diffraction (XRD)	Shimadzu XRD 6000	To study the crystallinity and crystallite size.

3.4 Overview of research methodology

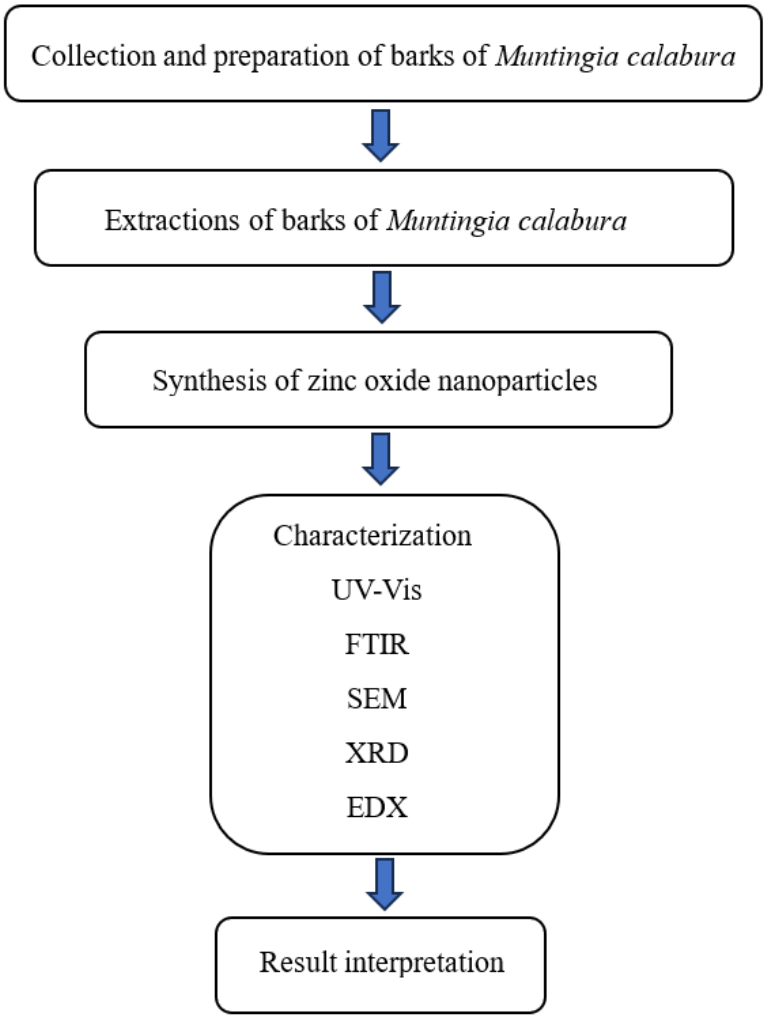

Figure 3.1: Overview of the study.

3.5 Experimental procedure

3.5.1 Collection and preparation of plant extracts

The barks of *M. calabura* were collected. The peeled barks were washed repeatedly with deionized water to remove impurities, dirt and soil. Then, the

washed barks were cut into small pieces and dried in the oven at 40 ℃ to remove moisture. The dried barks were grinded into powder form and stored in 50 mL centrifuge tube. The tube was sealed with parafilm and stored in desiccator for later use. To prepare *M. calabura* aqueous extract, 5 g of *M. calabura* barks powder was weighed using analytical balance and was added into 200 mL of deionized water. The mixture was heated at 80 – 100 ℃ for 30 minutes using a hot plate with constant stirring. The extract was allowed to cool to room temperature and was centrifuge at the speed of 6000 rpm for 10 minutes. The aqueous extract obtained was stored in the refrigerator at 4 ℃ for further use. Figure 3.2 shows the process flowchart for the preparation of *M. calabura* extract.

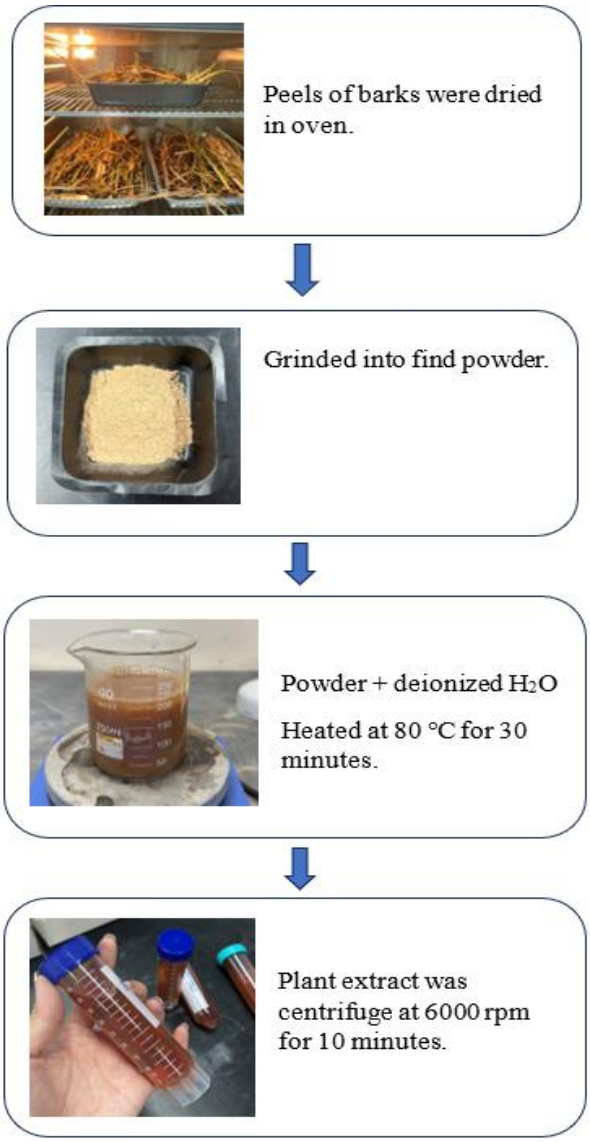

Figure 3.2: Process flowchart to prepare the *M. calabura* extract.

3.5.2 Green synthesis of zinc oxide nanoparticles

Twenty mL of extract was heated to 80 °C with constant stirring followed by the addition of 2 g of zine nitrate hexahydrate into the 20 mL extract dropwise. The mixture was heated with constant stirring until a brown paste was formed. The paste was transferred to a ceramic crucible and calcinated at 450 °C for 2 hours

in the furnace. Fine and white ZnO powder was obtained and stored in a seal airtight micro sample tube in the desiccator for further characterization. Figure 3.3 demonstrates the process flowchart for synthesis of ZnO NPs.

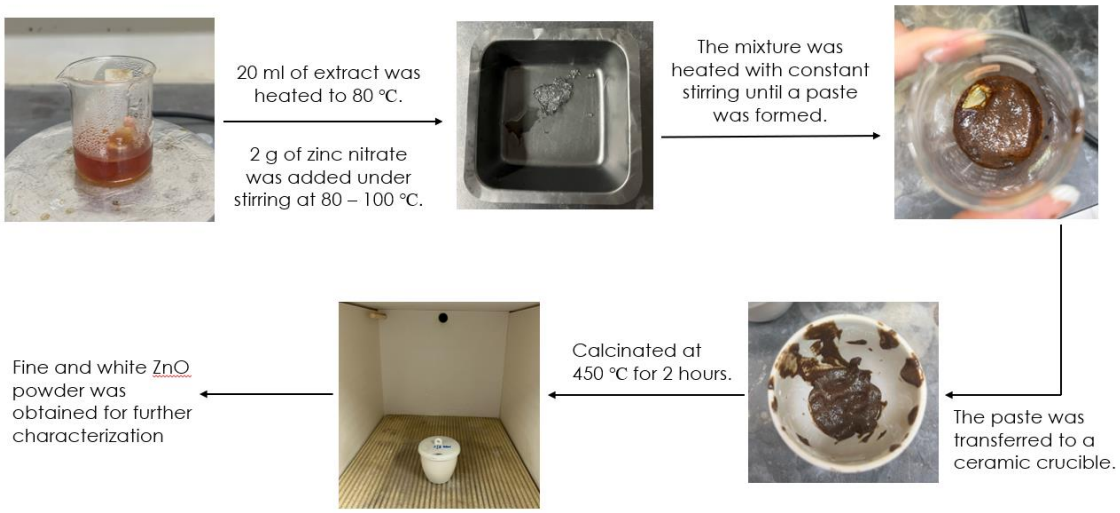

Figure 3.3: Process flowchart for synthesis of ZnO NPs.

3.6 Yield of synthesized zinc oxide nanoparticles

The mass of the salt precursor used and the final product, synthesized ZnO NPs were weighed using an analytical weighing balance. The percentage yield of the synthesized zinc oxide nanoparticles was calculated using Equation 3.1.

$$\text{Percentage yield of ZnO NPs} = \frac{Mass\ of\ ZnO\ NPs}{Mass\ of\ Zn(NO_3)_2.6H_2O} \times 100\% \quad \text{---- Equation 3.1}$$

3.7 Characterization of synthesized ZnO NPs

The synthesized ZnO NPs were characterized by using Fourier Transform Infrared Spectroscopy (FTIR), Ultraviolet-Visible (UV-Vis) Spectroscopy, X-ray Diffraction (XRD), Scanning Electron Microscope (SEM), and Energy Dispersive X-Ray Spectroscopy (EDX).

3.7.1 Fourier Transform-Infrared Spectroscopy (FTIR)

The functional groups of *M.calabura* extract and synthesized ZnO NPs were determined using Perkin Elmer Spectrum RX1 Fourier Transform-Infrared Spectrometer along with potassium bromide, KBr pellet technique. The model of spectrometer is shown in Figure 3.4. The scanning range is from 4000 cm^{-1} to 400 cm^{-1}. To determine the presence of functional groups in the plant extract, the aqueous extract was freeze fried using freeze dryer before subjected to FTIR analysis. The determination of ZnO NPs was achieved by mixing the synthesized ZnO NPs with KBr by using mortar and pestle to grind into fine powder. The FTIR spectra of *M.calabura* extract was compared with the synthesized ZnO NPs.

Figure 3.4: Perkin Elmer Spectrum RX1 model.

3.7.2 Ultraviolet-Visible Spectroscopy (UV-Vis)

The optical properties of ZnO NPs were studied using Thermo Fisher Scientiffic Genesys 180 Series UV-Visible Spectrophotometer and the scanning is from 200 to 1000 nm using deionized water as blank. The sample solution was prepared by dispersing 5 mg of ZnO NPs into 10 mL deionized water in a 15 mL centrifuge tube and sonicated for 10 minutes at room temperature.

Figure 3.5: Thermo Fisher Scientific Genesys 180 series.

After obtaining the maximum absorption peak of ZnO NPs, the band gap energy could be calculated using Equation 3.2. The formation of ZnO NPs could be further confirmed by the band gap energy.

$$\text{Band gap energy, } E_{bg} = \frac{hc}{\lambda} \qquad \text{--------- Equation 3.2}$$

Where,

h = Planck's constant (6.626×10^{-34} Js)

c = Speed of light (3.00×10^{8} ms^{-1})

λ = Maximum absorption wavelength (nm)

The band gap energy value obtained is in the unit of Joule (J). Hence, conversion factor is required to convert J to electron volt (eV) to determine the amount of energy gained by an electron to be excited by an electric potential difference of one volt.

$$1 \text{ eV} = 1.602 \times 10^{-19} \text{ J}$$

3.7.3 Field Emission Scanning Electron Microscopy (FESEM) and Energy Dispersive X-ray Spectroscopy (EDX)

The SEM-EDX analysis was carried out to determine the surface morphology, shape of the synthesized ZnO NPs using Scanning Electron Microscopy (JEOL JSM-6710F) with emission current of 4.0 kV and to study the elemental

composition using energy dispersive x-ray spectroscopy (Oxford Instruments X-Max 50mm^2).

Figure 3.6: JEOL JSM-6701F SEM-EDX.

3.7.4 X-ray Diffraction (XRD)

The crystalline structure and crystallite size of synthesized ZnO NPs was determined using X-ray Diffractometer (Shimadzu XRD 6000) with Cu K_α radiation (λ = 1.5406 Å) over a 2θ range from 10° to 70° at a scanning rate of 0.05 cm^{-1}. The peaks observed were compared to the International Centre for Diffraction Data (ICDD card No. 01-071-6424). The crystallite sized obtained were calculated using Debye Scherrer equation as shown in Equation 3.3.

$$D = \frac{K\lambda}{\beta \cos\theta}$$ ---------- Equation 3.3

Where,

D = Crystallite size in diameter

K = Scherrer constant, 0.9

λ = Wavelength of X-ray source (Cu K_α radiation= 1.5406 Å)

β = Full width at half maximum (FWHM) of the diffraction peak in radian 2θ

θ = Bragg's angle of diffraction

β obtained can be calculated by using equation:

$$\beta = \frac{\text{FWHM in } 2\theta \times \pi}{180^\circ}$$ ---------- Equation 3.4

Figure 3.7: Shimadzu XRD 6000.

CHAPTER 4

RESULTS AND DISCUSSION

4.1 Green Synthesis of ZnO nanoparticles

In this study, ZnO NPs were synthesized through the green synthesis pathway by using the bark extract of *M. calabura*. The approach involved in the synthesis was bottom-up approach along with the zinc nitrate hexahydrate, $Zn(NO_3)_2.6H_2O$ as the precursor salt. There are several phytochemicals present in the plant extract such as flavonoids, alkaloids, polyphenols and many more. They served as the reducing and stabilizing agent for the reduction of zinc ions, Zn^{2+} to its metallic form, Zn (Thatyana et al., 2023). The reduction process could be confirmed by observing the colour change of the solution from light brown to dark brown and slowly into dark brown paste form. The observation of the reduction process is shown in Figure 4.1.

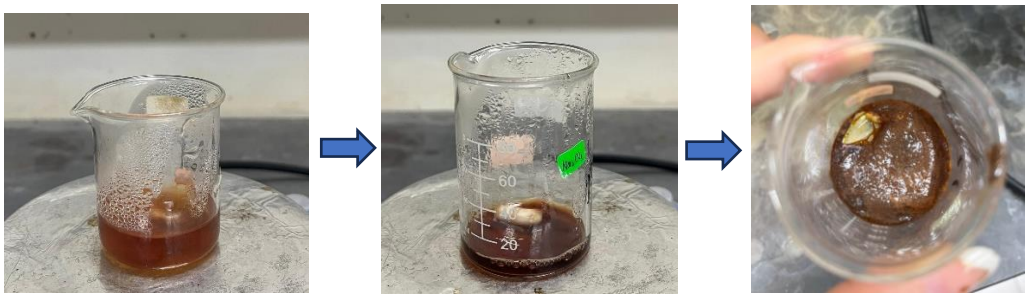

Figure 4.1: Reduction of Zn^{2+} to elemental Zn from light brown to dark brown and slowly into paste form.

Zinc nitrate hexahydrate served as the source for the zinc in this study. During the synthesis process, the heating temperature of bark extract must be properly controlled. It was heated to 80 ℃ and the temperature range was controlled within 80 to 100 ℃. This is because organic compounds that present in the barks might be decomposed at high temperatures. The dissolved zinc nitrate hexahydrate was added dropwise into the bark extract with constant stirring to ensure homogenous mixing and to ensure the uniformity of the shape of ZnO NPs formed. During the heating process, the light brown solution slowly turned into darker brown and slowly the solution turned to a dark brown colour paste. Reduction was occurred in this process where the zinc salt, Zn^{2+} was reduced to zinc, Zn. Finally, a white powder was obtained after calcination.

In this reaction, there are two proposed mechanisms which are through the bio-reduction or chelation process (Weldegebrieal, 2020). In bio-reduction, the phytochemicals (PC) in the bark extract reduced the Zn^{2+} into elemental Zn. During calcination, the phytochemicals would be degraded at high temperature leaving the Zn to react with oxygen. Hence, reaction of Zn with oxygen occurred to form ZnO NPs. The reaction is presented by Equations 4.1 and 4.2.

$$Zn^{2+} + PC \rightarrow Zn + PC\ (oxidized) \quad \text{---------- Equation 4.1}$$

$$Zn + O_2 \rightarrow ZnO \quad \text{---------- Equation 4.2}$$

In chelation process, Zn^{2+} formed a complex with the phytochemicals (PC) and the complex was stabilized by the PC. The formation of complex was through the polar functional groups of PC such as -OH, -COOH and -C=O. Next, the complex would be subject to calcination and thermally decomposed to release ZnO NPs as shown by Equations 4.3 and 4.4.

$$Zn^{2+} + PC \rightarrow Zn\text{-}PC \text{ (complex)} \qquad \text{---------- Equation 4.3}$$

$$Zn - PC \text{ (complex)} \xrightarrow{\Delta} ZnO \qquad \text{---------- Equation 4.4}$$

The methodologies employed in this study is a green approach as it fulfilled the principles of green chemistry. The bark extract served as the green source, and it is renewable while the phytochemicals acted as the green reducing agent where pollution can be prevented as no harmful and hazardous waste will be generated. In addition, the reaction did not involve the use of harmful chemicals and the reaction was conducted under mild conditions. Safer solvent and chemicals were used such as deionized water. Deionized water is a green solvent as it is non-toxic, cheap and easily available. In addition, zinc nitrate hexahydrate was used as the precursor salt as it is cost effective, readily available which makes it to be a convenient choice for the green synthesis process. Most importantly, zinc nitrate is environmentally friendly compared to other toxic chemicals. Overall, the procedure carried out in this study fulfilled the requirement of green chemistry which is able to enhance the sustainability by minimizing environmental impacts.

4.2 Characterization of Synthesized Zinc Oxide Nanoparticles

The white coloured powder of ZnO NPs synthesized was characterized by using Fourier Transform Infrared Spectroscopy (FTIR), Ultraviolet-Visible (UV-Vis) Spectroscopy, X-ray Diffraction (XRD), Scanning Electron Microscope (SEM), and Energy Dispersive X-Ray Spectroscopy (EDX).

4.2.1 Fourier-Transform Infrared Spectroscopy (FTIR)

The FTIR analysis was scanned in the range of wavenumber from 4000 to 400 cm^{-1} to detect the presence of functional groups in the synthesized ZnO NPs and in the *M. calabura* bark extract. Figure 4.2(a) shows the FTIR spectrum of the *M. calabura* bark extract. The broad absorption peak observed at 3431 corresponding to the O-H bond of the polyphenols. However, some of the background impurities were present in the spectrum such as the atmospheric component carbon dioxide, CO_2 which could be found at around 2360 cm^{-1} and 2342 cm^{-1}. These two doublet peaks corresponding to the asymmetric stretching mode of carbon dioxide (Pavia et al., 2009). During the process of grinding the sample with KBr, some of the moisture and carbon dioxide might be absorbed by the KBr and appeared as the impurities in the spectrum. The C=O stretching of flavonoids could be observed at 1617 cm^{-1}. Moreover, the C-C stretching of aromatic ring were represented by the peak at 1448 cm^{-1} (Golmohammadi, Honarmand and Ghanbari, 2020). The peak located at 1354 cm^{-1} corresponding to the COO^- stretching of the carboxylic acid. The C-O stretching and C-N amine

stretching of alkaloids could be observed at 1232 cm^{-1} and 1038 cm^{-1} respectively (Selvanathan et al., 2021).

Based on Figure 4.2(b) which shows the FTIR spectrum of synthesized ZnO NPs, the intense peak at 3448 cm^{-1} indicated the O-H stretching of the phenolic compounds. In addition, the spectrum showed a peak at around 1636 cm^{-1} due to the C=O stretching of flavonoids. Furthermore, the COO^- stretching of carboxylic acid could be found at 1384 cm^{-1}. Lastly, the formation of ZnO NPs were shown at 459 cm^{-1} due to the Zn-O stretching. Based on the two spectrum as shown in Figure 4.2(a) and Figure 4.2(b), the shifting of peaks were observed in the FTIR spectrum of synthesized ZnO NPs such as 3431 – 3448 cm^{-1}, 1617 – 1636 cm^{-1}, 1354 – 1384 cm^{-1} indicated that the phytochemicals such as phenols, flavonoids and other phytochemicals that are having the functional groups O-H, C=O, COOH, C-N were involved in the reaction to synthesize the ZnO NPs (Aminuzzaman et al., 2018). In both of the spectrum observed, the C=O was shifted to lower frequency due to the conjugation of aromatic ring. However, the synthesized ZnO NPs were not completely pure due to the presence of impurities such as the organic compounds were not decomposed completely.

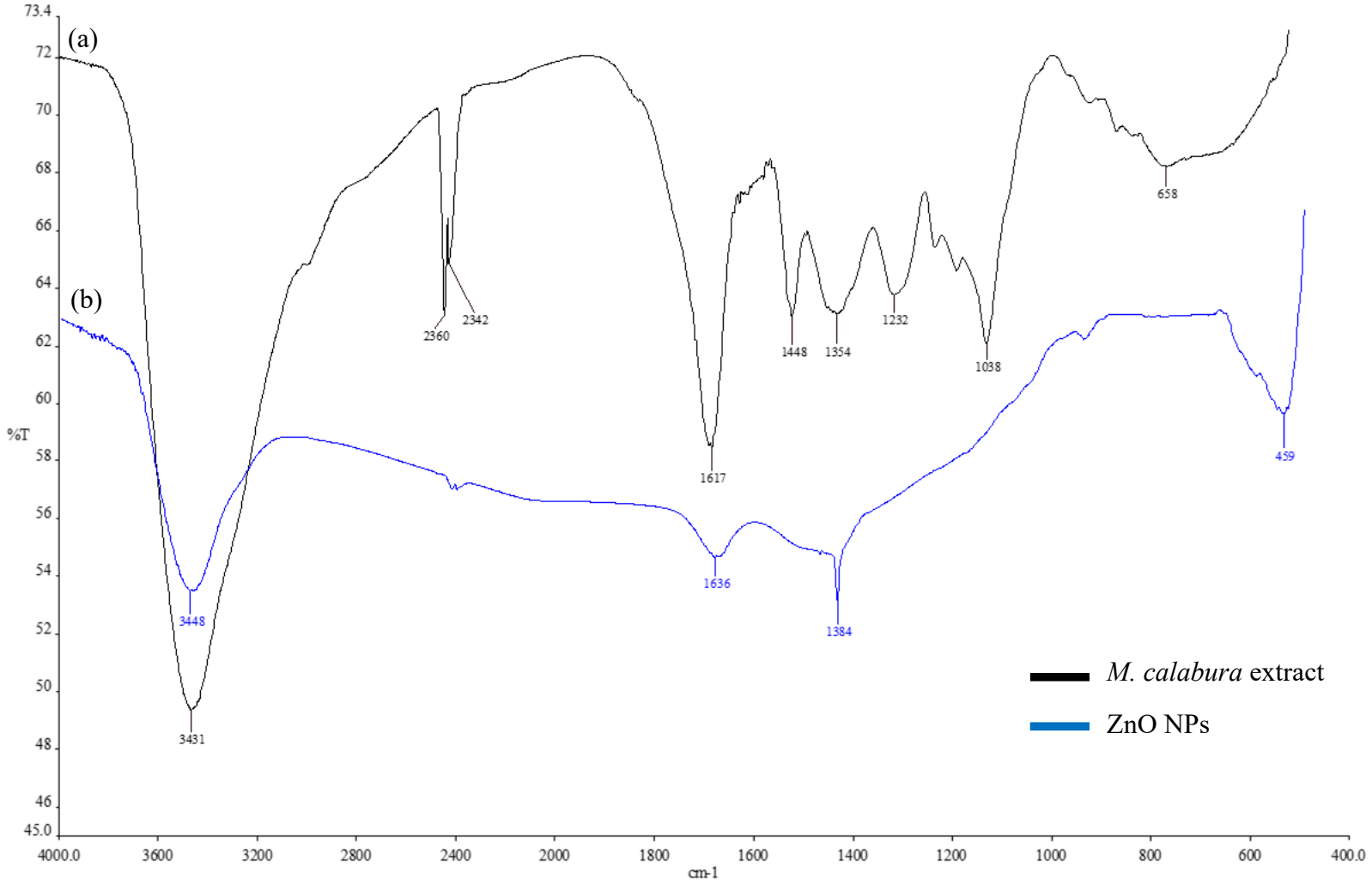
(a)
(b)
%T
cm-1
3431
3448
2360
2342
1617
1636
1448
1354
1384
1232
1038
658
459
M. calabura extract
ZnO NPs

Figure 4.2: FTIR spectrum of (a) aqueous extract of bark of *M. calabura*, (b) synthesized ZnO NPs.

Table 4.1: Summary of FTIR spectra of bark extract of *M. calabura* and ZnO NPs.

Muntingia calabura bark extract		Zinc oxide nanoparticles	
Wavenumber (cm^{-1})	Predicted vibrational mode	Wavenumber (cm^{-1})	Predicted vibrational mode
3431	O-H stretching	3448	O-H stretching
2342, 2360	O=C=O stretching	1636	C=O stretching
1617	C=O stretching	1384	COO^- stretching
1448	C-C stretching of aromatic ring	459	Zn-O stretching
1354	COO^- stretching		
1232	C-O stretching		
1038	C-N stretching		

4.2.2 Ultraviolet-Visible Spectroscopy (UV-Vis)

Ultraviolet-Visible spectroscopy was used to determine the absorption value of the synthesized ZnO NPs. Absorption spectroscopy is a non-destructive technique to exploit the optical properties of semiconducting nanoparticles. The UV-Vis absorption spectrum is a function of wavelength and the maximum wavelength, λ_{max} will affect the size of the nanoparticle (Mohammadian, Es'haghi, and Hooshmand, 2018). The absorption spectrum of ZnO NPs was measured from 300 to 800 nm wavelength. Based on the absorption spectrum, the maximum absorption peak of ZnO NPs was detected at 373 nm as shown in Figure 4.3. This absorption peak of ZnO NPs at 373 nm is aligned with the research conducted by Mohammadian and his coworkers (2018) on the characterization of zinc oxide nanoparticles and size evaluation by UV-Vis spectroscopy.

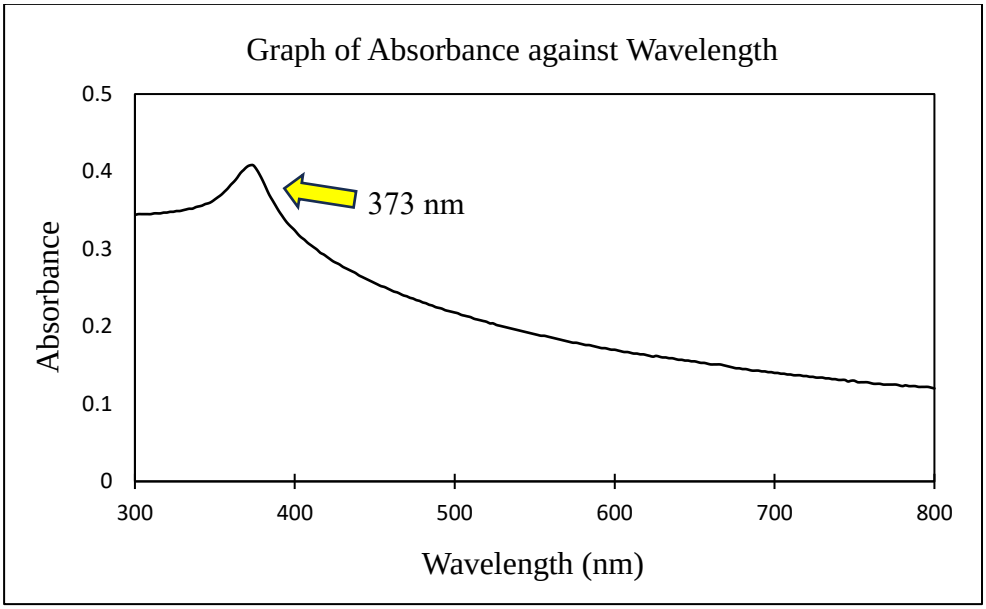

Figure 4.3: Absorption spectrum of synthesized ZnO NPs from 300 nm to 800 nm.

In addition, the appearance of the maximum absorption peak in the UV-Vis spectrum is attributed to the surface plasmon resonance (SPR) effect. SPR refers to the phenomenon where the absorption peak appears in the spectrum due to the oscillation of conduction electrons on the NPs surface when they have the appropriate energy. The resonant energy exhibits as a peak in the spectrum and this depends on the size, shape and the material of the NPs (Soliman et al., 2017).

The band gap energy is determined by the energy difference between the valence band and the conduction band. Therefore, this band gap energy refers to the minimum change in energy needed to excite an electron. The value obtained from the maximum absorption wavelength could be used to determine the band gap energy of the synthesized ZnO NPs. By using Equation 3.2, the calculated band gap energy of the synthesized ZnO NPs was 3.32 eV which is in accordance with the band gap energy value obtained by Khamis, Gouda and Nagiub (2023). This proves the presence of the ZnO NPs formation.

The band gap energy value obtained in this study was lower than the band gap energy of the bulk ZnO that had a band gap of 3.2 eV with a maximum wavelength of 387 nm (Nawaz et al., 2011). This is due to the blue shifting behaviour of the bulk ZnO (387 nm) to nanosized ZnO (373 nm) which resulted in higher energy and lower wavelength. This blue shift is due to the quantum confinement effect that resulted in decreasing in size of the ZnO NPs as the energy band gap increased and the decreased in wavelength. Quantum confinement effect can be explained more clearly through the illustration as

shown in Figure 4.4 where the band gap increases with the decrease in the size of NPs (Mohamed et al., 2021).

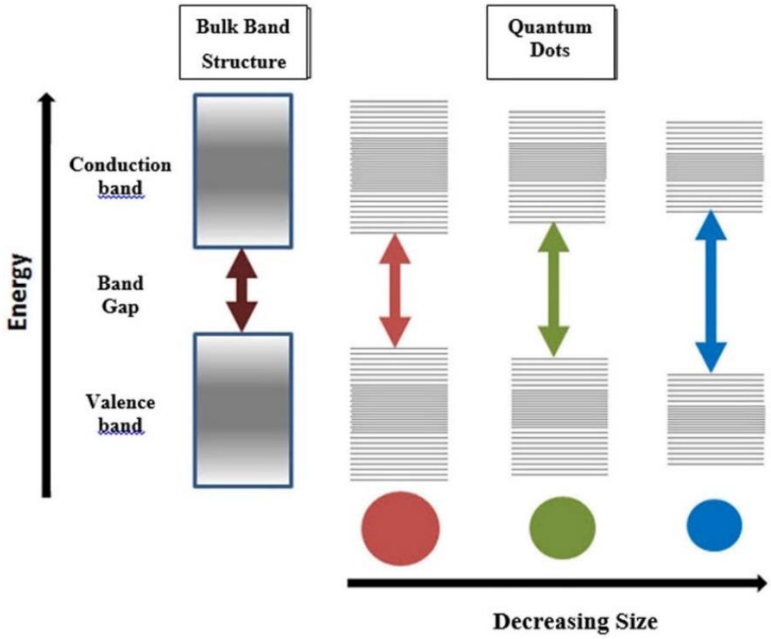

Figure 4.4: Splitting of band gap energy due to quantum confinement effect (Mohamed et al., 2021).

4.2.3 Field Emission Scanning Electron Microscopy (FESEM)

The surface morphology, size and shape of the green synthesized ZnO NPs were determined by scanning electron microscopy at different magnifications as shown Figure 4.5. Based on the SEM images, the synthesized ZnO NPs exhibit a spherical shape and agglomeration was observed. This is because the smaller size of particles possessed high surface energy. As a result, the increased surface energy contributes to greater potential for agglomeration to occur (Safardoust-Hojaghan et al., 2021). In addition, the agglomeration could also be due to the

electrostatic attraction and polarity of the nanoparticles (Aminuzzaman et al., 2018). According to the SEM particle analysis, the size of the ZnO NPs were found to be in the range of 38.0 – 71.4 nm as shown in Figure 4.5 (d).

(a)

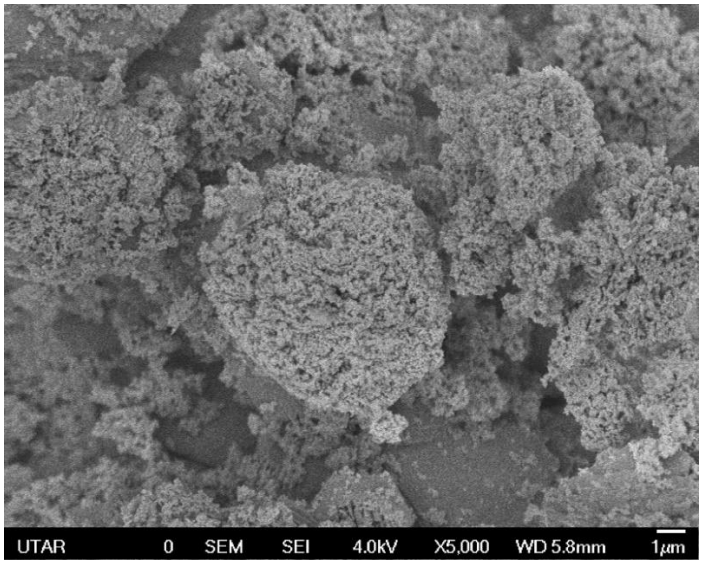

(b)

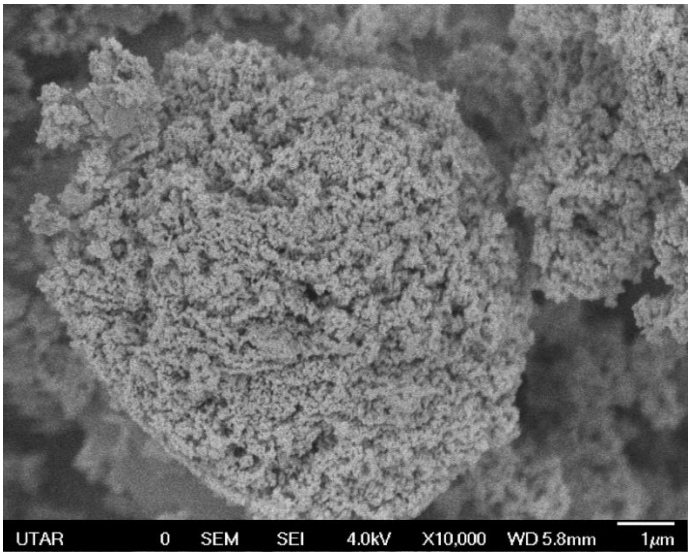

Figure 4.5: FESEM image of ZnO NPS at magnification of (a) 5000× (b) 10000×.

(c)

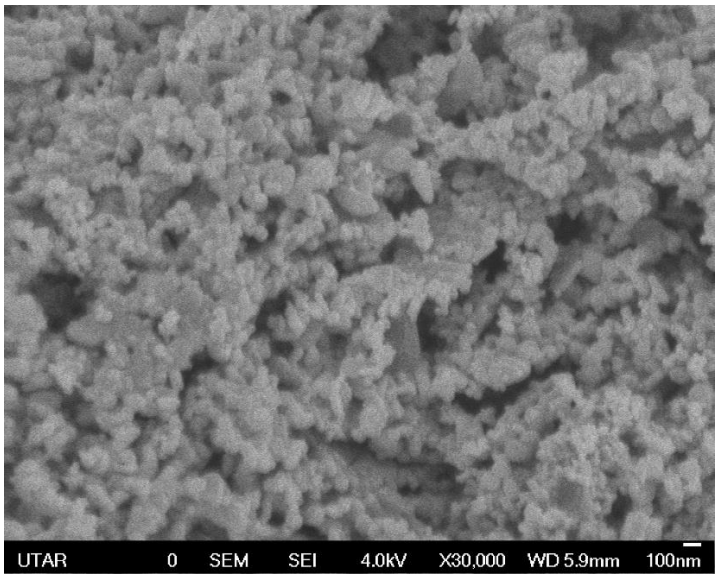

(d)

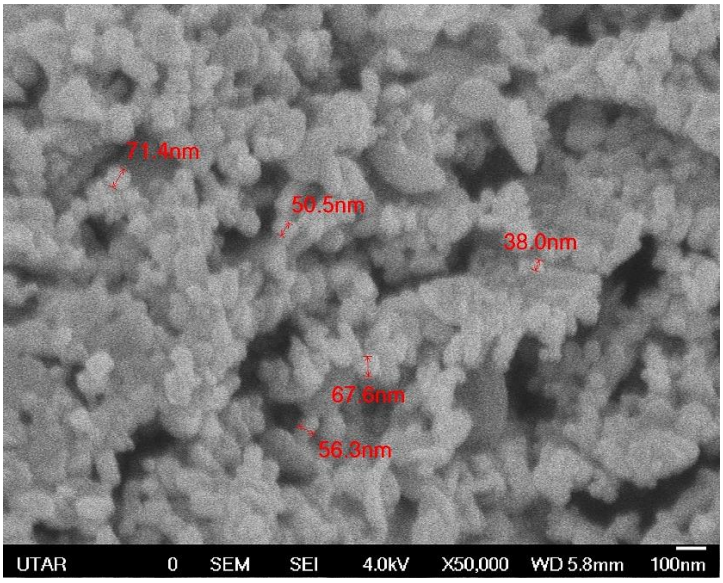

Figure 4.5: FESEM image of ZnO NPS at magnification of (c) 30000× (d) 50000×.

4.2.4 Energy Dispersive X-ray Spectroscopy (EDX)

EDX spectroscopy was carried out to determine the elemental composition of the ZnO NPs.

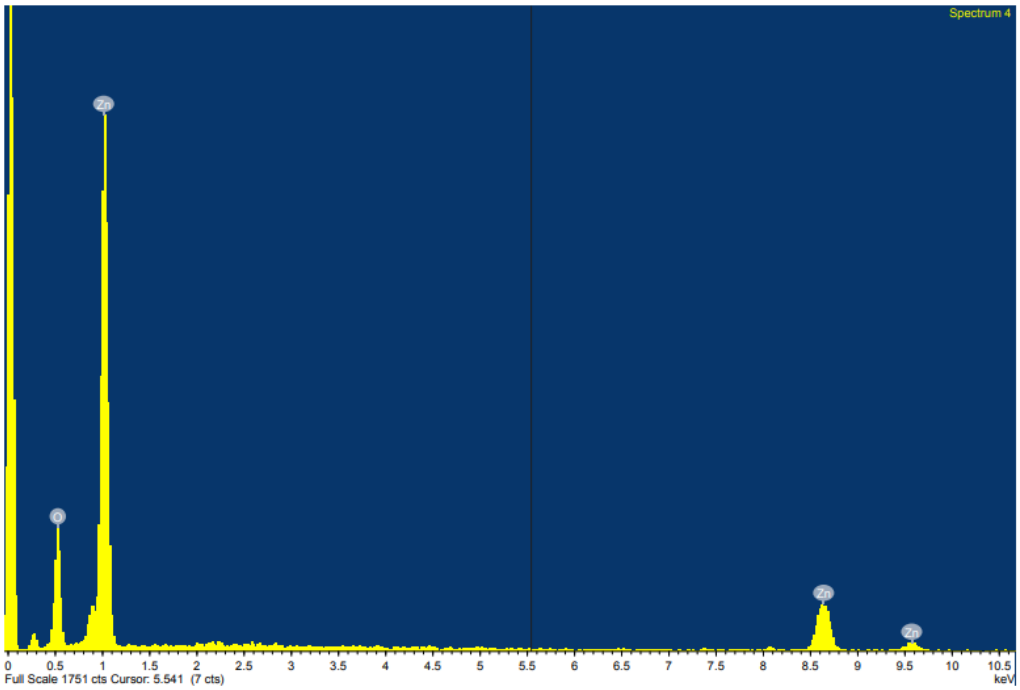

Figure 4.6: EDX spectrum of green synthesized ZnO NPs.

Table 4.2: EDX analysis of weight percent and atomic percent of the elements present in ZnO NPs.

Element	Weight percent (%)	Atomic percent (%)
Zinc (Zn)	57.93	25.20
Oxygen (O)	42.07	74.80
Total	100.00	100.00

Based on the EDX spectrum in Figure 4.6, the elements that present in the ZnO NPs are Zn and O with a weight percent of 57.93% and 42.07% respectively as summarized in Table 4.2. The presence of Zn and O peaks in the spectrum proved the formation of ZnO NPs. In addition, the absence of any foreign particles and impurities in the EDX spectrum confirms the purify of ZnO NPs produced by the *M. calabura* bark extract. It can be observed that there is a peak located at 0 keV. This peak is referred to as the noise peak or the zero-energy strobe peak. This strobe peak served as a reference peak corresponding to zero energy (Statham, 2002). In this case, the threshold settings have to be adjusted in order to minimize the occurrence of the zero-energy peak.

4.2.5 X-ray Diffraction (XRD)

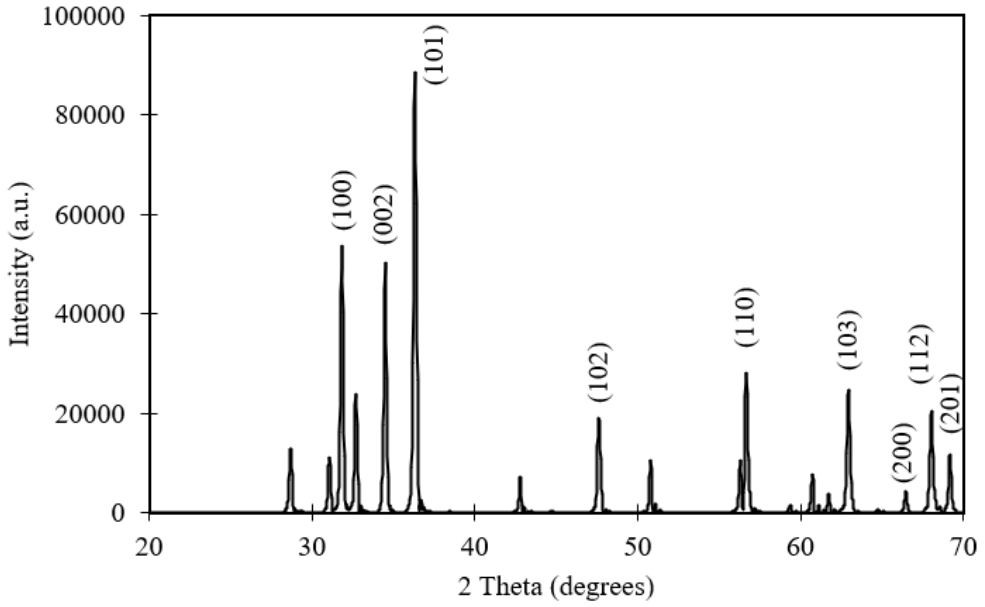

Figure 4.7: XRD diffractogram of green synthesized ZnO NPs.

Table 4.3: Crystallite size distribution based on Debye-Scherrer's equation.

2θ	Miller's index	FWHM (°)	β(radians)	D (nm)
31.92	(100)	0.20	0.00349	41.31
34.58	(002)	0.20	0.00349	41.60
36.41	(101)	0.16	0.00279	52.27
47.70	(102)	0.16	0.00279	54.29
56.75	(110)	0.16	0.00279	56.43
63.02	(103)	0.20	0.00349	46.59
66.53	(200)	0.16	0.00279	59.38
68.11	(112)	0.24	0.00419	39.95
69.25	(201)	0.20	0.00349	48.27

The crystallite size and structure of ZnO NPs synthesized from the *M. calabura* bark extract could be studied by XRD. The intensity of the peak indicates the position of atoms within the lattice structure while the crystallite size of the NPs can be determined from the peak width. Miller indices (hkl) is a set of system that identify the crystallographic plane or surface (Nix, 2022). Based on the XRD spectrum of the synthesized ZnO NPs as shown in Figure 4.7, the diffraction peaks at 2θ were detected at 31.92°, 34.58°, 36.41°, 47.70°, 56.75°, 63.02°, 66.53°, 68.11°, 69.25° which corresponded to the crystal lattice planes of (100), (002), (110), (103), (200), (112), (201) respectively. These diffraction peaks were 87.8% matched with the standard card of The International Centre for Diffraction Data (ICDD) Card No. 01-071-6424 shown in Appendix F to H that suggesting the hexagonal wurtzite structure of ZnO NPs phase with a space group of $P6_3mc$. The lattice parameter was found to be a = 3.2494 Å and c = 5.2038 Å.

The crystalline nature of ZnO NPs could be indicated by the intense diffraction peaks. The degree of crystallinity of the synthesized ZnO NPs was 19.39%. This low crystallinity might be due to large amount of amorphous content and the occurrence of peaks broadening in the diffractogram. Based on the XRD analysis, there were some unrelated and unmatched peaks which could be found in the diffractogram indicated the presence of some impurities. The degree of purity would be affected by the presence of impurities. The crystallite size of the synthesized ZnO NPs was determined from the full width at half maximum (FWHM) of the diffraction peaks using Debye-Scherrer equation as shown in Appendix B. The average crystallite size was found to be 48.90 nm.

Similar research reported by Umamaheswari et al. (2021) where the diffraction peaks were located at 30.10°, 33.91°, 36.60°, 44.10°, 56.56°, 60.00°, 65.10°, 69.10°, and 70.48° were indexed to (100), (002), (101), (102), (110), (103), (200), (112), and (201) respectively and were attributed to hexagonal wurtzite structure. Debye Scherrer equation was used to calculate the average crystallite size of ZnO NPs which was reported to be 33.01 nm.

CHAPTER 5

CONCLUSION

5.1 Conclusion

In this study, zinc oxide nanoparticles (ZnO NPs) were successfully synthesized by the green synthesized route with the aid of the bark extract of Malayan Cherry (*Muntingia calabura)* and the zinc nitrate hexahydrate as the salt precursor. This is a remarkable finding because there has been limited research conducted on synthesis of nanoparticles using the bark where most of the researchers focus on utilizing the leaves instead. The findings revealed that the phytochemicals in the bark extract of *Muntingia calabura* were involved in the reaction by acting as the reductant and stabilizer in synthesizing the ZnO NPs. The green synthesized ZnO NPs were characterized by FT-IR, UV-Vis, FESEM, EDX and XRD.

It was concluded that the ZnO NPs showed an intense peak at 459 cm^{-1} in the FTIR spectrum which indicated the Zn-O stretching vibration. In UV-Vis analysis, it has a maximum absorption wavelength at 373 nm with a band gap energy of 3.32 eV. In addition, the FESEM images showed that the morphology of ZnO NPs having a spherical shape with a particle size ranging from 38.0 – 71.4 nm. The elemental composition of ZnO NPs was determined by EDX, it proved that the elements that present in the EDX spectrum were zinc and oxygen with a weight percent of 57.93% and 42.07% respectively. The XRD diffractogram showed ZnO NPs has a hexagonal wurtzite structure with crystalline nature and a crystallite size of 48.90 nm.

5.2 Further studies

It is suggested to carry out future studies in this project. Firstly, phytochemicals screening test of the bark extract could be studied to ascertain the specific phytochemicals that present in the extract. Moreover, the synthesized ZnO NPs could be further characterized by transmission electron microscopy (TEM), photoluminescence (PL) spectroscopy and Raman spectroscopy. Additionally, the synthesized ZnO NPs could be utilized in various applications such as in the biological study or in the photocatalytic degradation of dye to evaluation its performance. Apart from that, the parameters such as the concentration of the plant extract, mass of precursor used, and calcination temperature could be investigated to determine their influence on the nanoparticles.

References

Abid, N., Khan, A.M., Shujait, S., Chaudhary, K., Ikram, M., Imran, M., Haider, J., Khan, M., Khan, Q. and Maqbool, M., 2022. Synthesis of nanomaterials using various top-down and bottom-up approaches, influencing factors, advantages, and disadvantages: A review. *Advances in Colloid and Interface Science*, [online] 300, p.102597. https://doi.org/10.1016/j.cis.2021.102597.

Ahmaruzzaman, M. and Raha, S., 2022. ZnO nanostructured materials and their potential applications: Progress, Challenges and Perspectives. *Nanoscale Advances*, (4). https://doi.org/10.1039/d1na00880c.

Aminuzzaman, M, Ng, P.S., Goh, W.S., Ogawa, S. and Watanabe, A., 2019. Value-adding to dragon fruit (*Hylocereus polyrhizus*) peel biowaste: green synthesis of ZnO nanoparticles and their characterization. *Inorganic and Nano-Metal Chemistry*, 49(11), pp.401–411. https://doi.org/10.1080/24701556.2019.1661464.

Aminuzzaman, M., Ying, L.P., Goh, W.-S. and Watanabe, A., 2018. Green synthesis of zinc oxide nanoparticles using aqueous extract of Garcinia mangostana fruit pericarp and their photocatalytic activity. *Bulletin of Materials Science*, 41(2). https://doi.org/10.1007/s12034-018-1568-4.

Anastas, P. and Warner, J., 1998. *12 Principles of Green Chemistry*. [online] American Chemical Society. Available at: <https://www.acs.org/greenchemistry/principles/12-principles-of-green-chemistry.html>

Ansori, A.N.M., Kharisma, V.D. and Solikhah, T.I., 2021. Medicinal properties of Muntingia calabura L.: A Review. *Research Journal of Pharmacy and Technology*, 14(8), pp.4509–4512. https://doi.org/10.52711/0974-360x.2021.00784.

Ashokkumar, K., Simal-Gandara, J., Murugan, M., Dhanya, M.K. and Pandian, A., 2022. Nutmeg (*Myristica fragrans* Houtt.) essential oil: A review on its composition, biological, and pharmacological activities. *Phytotherapy Research*, 36(7), pp.2839–2851. https://doi.org/10.1002/ptr.7491.

Bayda, S., Adeel, M., Tuccinardi, T., Cordani, M. and Rizzolio, F., 2019. The History of Nanoscience and Nanotechnology: From Chemical–Physical Applications to Nanomedicine. *Molecules*, [online] 25(1), p.112. https://doi.org/10.3390/molecules25010112.

Bhardwaj, K., Dubey, W., Correspondence, K. and Bhardwaj, 2019. Quantitative analysis of primary and secondary metabolites of ethanol seed extract of Origanum majorana (Marjoram). *~ 1251 ~ Journal of Pharmacognosy and Phytochemistry*, [online] 8(1), pp.1251–1255. Available at <ttps://www.phytojournal.com/archives/2019/vol8issue1/PartU/7-6-551-580.pdf>

Bionutricia, D., 2023. *Soursop Fruit (Annona muricata)*. Bionutricia Extract. [online] Available at: <https://bionutriciaextract.com/knowledge-soursop-fruit-annona-muricata/>

Darvishi, E., Kahrizi, D. and Arkan, E., 2019. Comparison of different properties of zinc oxide nanoparticles synthesized by the green (using Juglans regia L. leaf extract) and chemical methods. *Journal of Molecular Liquids*, 286, p.110831. https://doi.org/10.1016/j.molliq.2019.04.108.

Dhatwalia, J., Kumari, A., Chauhan, A., Mansi, K., Thakur, S., Saini, R.V., Ishita Guleria, Lal, S., Kumar, A., Khalid Mujasam Batoo, Byung Hyune Choi, Manicum, A.-L.E. and Kumar, R., 2022. Rubus ellipticus Sm. Fruit Extract Mediated Zinc Oxide Nanoparticles: A Green Approach for Dye Degradation and Biomedical Applications. *Materials*, [online] 15(10), pp.3470–3470. https://doi.org/10.3390/ma15103470.

Dréno, B., Alexis, A., Chuberre, B. and Marinovich, M., 2019. Safety of titanium dioxide nanoparticles in cosmetics. *Journal of the European Academy of Dermatology and Venereology: JEADV*, [e-journal] 33 (7), pp.34–46. https://doi.org/10.1111/jdv.15943.

Espitia, P.J.P., Soares, N. de F.F., Coimbra, J.S. dos R., de Andrade, N.J., Cruz, R.S. and Medeiros, E.A.A. (2012). Zinc Oxide Nanoparticles: Synthesis, Antimicrobial Activity and Food Packaging Applications. *Food and Bioprocess Technology*, 5(5), pp.1447–1464. https://doi.org/10.1007/s11947-012-0797-6.

Faisal, S., Jan, H., Shah, S.A., Shah, S., Khan, A., Akbar, M.T., Rizwan, M., Jan, F., Wajidullah, Akhtar, N., Khattak, A. and Syed, S., 2021. Green Synthesis of Zinc Oxide (ZnO) Nanoparticles Using Aqueous Fruit Extracts of Myristica fragrans: Their Characterizations and Biological and Environmental Applications. *ACS Omega*, 6(14), pp.9709–9722. https://doi.org/10.1021/acsomega.1c00310.

Flora & Fauna Web., 2020. *NParks | Cinnamomum verum*. [online] www.nparks.gov.sg. Available at: <https://www.nparks.gov.sg/florafaunaweb/flora/2/8/2807>

Flora & Fauna Web., 2021. *NParks | Muntingia calabura*. [online] Nparks.gov.sg. Available at: <https://www.nparks.gov.sg/florafaunaweb/flora/3/0/3036>

Golmohammadi, M., Honarmand, M. and Ghanbari, S., 2020. A green approach to synthesis of ZnO nanoparticles using jujube fruit extract and their application in photocatalytic degradation of organic dyes. *Spectrochimica Acta Part A: Molecular and Biomolecular Spectroscopy*, 229, p.117961. https://doi.org/10.1016/j.saa.2019.117961.

Govaerts, R., Nic Lughadha, E., Black, N., Turner, R. and Paton, A., 2021. The World Checklist of Vascular Plants, a continuously updated resource for exploring global plant diversity. *Scientific Data*, 8(1). https://doi.org/10.1038/s41597-021-00997-6.

H. Alshammari, B., A. Lashin, M.M., Adil Mahmood, M., S. Al-Mubaddel, F., Ilyas, N., Rahman, N., Sohail, M., Khan, A., Shukhratovich Abdullaev, S. and Khan, R., 2023. Organic and inorganic nanomaterials: fabrication, properties and applications. *RSC Advances*, [online] 13(20), pp.13735–13785. https://doi.org/10.1039/D3RA01421E.

Jobie, F.N., Ranjbar, M. and Moghaddam, A.H., 2021. Green synthesis of zinc oxide nanoparticles using Amygdalus scoparia Spach stem bark extract and their applications as an alternative antimicrobial, anticancer, and anti-diabetic agent. *Advanced Powder Technology*, 32(6), pp.2043–2052. https://doi.org/10.1016/j.apt.2021.04.014.

Joudeh, N. and Linke, D., 2022. Nanoparticle classification, physicochemical properties, characterization, and applications: a comprehensive review for biologists. *Journal of Nanobiotechnology*, 20(1). https://doi.org/10.1186/s12951-022-01477-8.

Juliana., 2022. *Green chemistry*. [online] Photoactive Nanomaterials. Available at: <https://photoactive-nanomaterials.pesquisa.ufabc.edu.br/research-topics/green-chemistry/>

Khamis, M., Gouda, G.A. and Nagiub, A.M., 2023. Biosynthesis approach of zinc oxide nanoparticles for aqueous phosphorous removal: physicochemical properties and antibacterial activities. *BMC chemistry*, 17(1). https://doi.org/10.1186/s13065-023-01012-2.

Lakshmipriya, T. and Gopinath, S.C.B., 2021. Introduction to nanoparticles and analytical devices. *Nanoparticles in Analytical and Medical Devices*, pp.1–29. https://doi.org/10.1016/b978-0-12-821163-2.00001-7.

Malik, S., Muhammad, K. and Waheed, Y., 2023. Nanotechnology: A Revolution in Modern Industry. *Molecules*, [online] 28(2), p.661. https://doi.org/10.3390/molecules28020661.

Marco, B.A., Rechelo, B.S., Tótoli, E.G., Kogawa, A.C. and Salgado, H.R.N., 2019. Evolution of green chemistry and its multidimensional impacts: A review. *Saudi Pharmaceutical Journal*, 27(1), pp.1–8. https://doi.org/10.1016/j.jsps.2018.07.011.

Mathew, S., 2020. Phytonanotechnology: A historical perspective, current challenges, and prospects. *Elsevier eBooks*, pp.1–20. https://doi.org/10.1016/b978-0-12-822348-2.00001-2.

Mohammadian, M., Es'haghi, Z., and Hooshmand, S., 2018. Green and chemical synthesis of zinc oxide nanoparticles and size evaluation by UV–vis spectroscopy. *Journal of Nanomedicine Research*, 7(1), pp.52–58. https://doi.org/10.15406/jnmr.2018.07.00175.

Mutakin, M., Fauziati, R., Fadhilah, F.N., Zuhrotun, A., Amalia, R. and Hadisaputri, Y.E., 2022. Pharmacological Activities of Soursop (Annona muricata Lin.). *Molecules*, [online] 27(4), p.1201. https://doi.org/10.3390/molecules27041201.

National Nanotechnology Initiative, 2022. *What Is So Special about 'Nano'? | National Nanotechnology Initiative*. [online] www.nano.gov. Available at: <https://www.nano.gov/about-nanotechnology/what-is-so-special-about-nano>

Nawaz, H.R., Solangi, B.A., Zehra, B. and Nadeem, U., 2011. Preparation of Nano Zinc Oxide and its Application inLeather as a Retanning and Antibacterial Agent. *Canadian Journal on Scientific and Industrial Research*, 2(4), pp. 164-170.

Nix, R., 2022. *4.3: Miller Indices (hkl)*. [online] Chemistry LibreTexts. Available at: <https://chem.libretexts.org/Courses/Lafayette_College/CHEM_440%3A_Structure_Determination/04%3A_X-ray_Crystallography/4.03%3A_Miller_Indices_(hkl)>

Ong, C.B., Ng, L.Y. and Mohammad, A.W., 2018. A review of ZnO nanoparticles as solar photocatalysts: Synthesis, mechanisms and applications. *Renewable and Sustainable Energy Reviews*, 81, pp.536–551. https://doi.org/10.1016/j.rser.2017.08.020.

Patra, J.K. and Baek, K.-H., 2014. Green Nanobiotechnology: Factors Affecting Synthesis and Characterization Techniques. *Journal of Nanomaterials*, 2014(6), pp.1–12. https://doi.org/10.1155/2014/417305.

Pavia , D.L., Lampman, G.M., Kriz, G.S. and Vyvyan, J.R., 2009. *Introduction to*. [online] Available at: <https://www.fkit.unizg.hr/_download/repository/Introduction_to_Spectroscopy_4e_by_Pavia.pdf>

Priya, G.T. and Yasmin, Y., 2022. Phytochemicals and Antibacterial Activity of Muntingia calabura Leaves Based Product. *Journal of Research in Medical and Dental Science*, 10(11), pp.259–263.

Pushpalatha, C., Suresh, J., Gayathri, V., Sowmya, S., Augustine, D., Alamoudi, A., Zidane, B., Mohammad Albar, N.H. and Patil, S., 2022. Zinc Oxide Nanoparticles: A Review on Its Applications in Dentistry. *Frontiers in Bioengineering and Biotechnology*, [online] 10. https://doi.org/10.3389/fbioe.2022.917990.

Roy, A., Elzaki, A., Tirth, V., Kajoak, S., Osman, H., Algahtani, A., Islam, S., Faizo, N.L., Khandaker, M.U., Islam, M.N., Emran, T.B. and Bilal, M., 2021. Biological Synthesis of Nanocatalysts and Their Applications. *Catalysts*, [online] 11(12), p.1494. https://doi.org/10.3390/catal11121494.

Safardoust-Hojaghan, H., Salavati-Niasari, M., Amiri, O., Rashki, S. and Ashrafi, M., 2021. Green synthesis, characterization and antimicrobial activity of carbon quantum dots-decorated ZnO nanoparticles. *Ceramics International*, 47(4), pp.5187–5197. https://doi.org/10.1016/j.ceramint.2020.10.097.

Selvanathan, V., Aminuzzaman, M., Tan, L.X., Win, Y.F., Guan Cheah, E.S., Heng, M.H., Tey, L.-H., Arullappan, S., Algethami, N., Alharthi, S.S., Sultana, S., Shahiduzzaman, M., Abdullah, H. and Aktharuzzaman, M., 2022. Synthesis, characterization, and preliminary in vitro antibacterial evaluation of ZnO nanoparticles derived from soursop (Annona muricata L.) leaf extract as a green reducing agent. *Journal of Materials Research and Technology*, 20, pp.2931–2941. https://doi.org/10.1016/j.jmrt.2022.08.028.

Shanmugam, K., Sellappan, S., Alahmadi, T.A., Almoallim, H.S., Natarajan, N. and Veeraraghavan, V.P., 2022. Green synthesized zinc oxide nanoparticles from Cinnamomum verum bark extract inhibited cell growth and induced caspase-mediated apoptosis in oral cancer KB cells. *Journal of Drug Delivery Science and Technology*, 74, p.103577. https://doi.org/10.1016/j.jddst.2022.103577.

Singh, J., Kumar, S., Alok, A., Upadhyay, S.K., Rawat, M., Tsang, D.C.W., Bolan, N. and Kim, K.-H., 2019. The potential of green synthesized zinc oxide nanoparticles as nutrient source for plant growth. *Journal of Cleaner Production*, 214, pp.1061–1070. https://doi.org/10.1016/j.jclepro.2019.01.018.

Sirelkhatim, A., Mahmud, S., Seeni, A., Kaus, N.H.M., Ann, L.C., Bakhori, S.K.M., Hasan, H. and Mohamad, D., 2015. Review on Zinc Oxide Nanoparticles: Antibacterial Activity and Toxicity Mechanism. *Nano-Micro Letters*, 7(3), pp.219–242. https://doi.org/10.1007/s40820-015-0040-x.

Soliman, M.G., Pablo del Pino, Parak, W.J. and Pelaz, B., 2017. Synthesis and Surface Engineering of Gold Nanoparticles, and Their Potential Applications in Bionanotechnology. *Elsevier eBooks*. https://doi.org/10.1016/b978-0-12-409547-2.12744-1.

Sponza, L., Jacek Goniakowski and Noguera, C., 2015. Structural, electronic, and spectral properties of six ZnO bulk polymorphs. *Physical Review B*, 91(7). https://doi.org/10.1103/physrevb.91.075126.

Statham, P.J., 2002. Limitations to accuracy in extracting characteristic line intensities from x-ray spectra. *Journal of Research of the National Institute of Standards and Technology*, 107(6), p.531. https://doi.org/10.6028/jres.107.045.

Surjushe, A., Vasani, R. and Saple, D., 2008. Aloe vera: A short review. *Indian Journal of Dermatology*, [online] 53(4), p.163. https://doi.org/10.4103/0019-5154.44785.

Thatyana, M., Dube, N.P., Kemboi, D., Manicum, A.-L.E., Mokgalaka-Fleischmann, N.S. and Tembu, J.V., 2023. Advances in Phytonanotechnology: A Plant-Mediated Green Synthesis of Metal Nanoparticles Using Phyllanthus Plant Extracts and Their Antimicrobial and Anticancer Applications. *Nanomaterials*, [online] 13(19), p.2616. https://doi.org/10.3390/nano13192616.

Umamaheswari, A., Prabu, S.L., John, S.A. and Puratchikody, A., 2021. Green synthesis of zinc oxide nanoparticles using leaf extracts of Raphanus sativus var. Longipinnatus and evaluation of their anticancer property in A549 cell lines. *Biotechnology Reports*, 29, p.e00595. https://doi.org/10.1016/j.btre.2021.e00595.

Virkutyte, J. and Varma, R.S., 2011. Green synthesis of metal nanoparticles: Biodegradable polymers and enzymes in stabilization and surface functionalization. *Chem. Sci.*, 2(5), pp.837–846. https://doi.org/10.1039/c0sc00338g.

Wang, D., Cui, L., Chang, X. and Guan, D., 2020. Biosynthesis and characterization of zinc oxide nanoparticles from Artemisia annua and investigate their effect on proliferation, osteogenic differentiation and mineralization in human osteoblast-like MG-63 Cells. *Journal of Photochemistry and Photobiology B: Biology*, 202, p.111652. https://doi.org/10.1016/j.jphotobiol.2019.111652.

Weldegebrieal, G.K, 2020. Synthesis method, antibacterial and photocatalytic activity of ZnO nanoparticles for azo dyes in wastewater treatment: a review. *Inorganic Chemistry Communications*, 120, p.108140. https://doi.org/10.1016/j.inoche.2020.108140.

Yasunaka, K., Abe, F., Nagayama, A., Okabe, H., Lozada-Pérez, L., López-Villafranco, E., Muñiz, E.E., Aguilar, A. and Reyes-Chilpa, R., 2005. Antibacterial activity of crude extracts from Mexican medicinal plants and purified coumarins and xanthones. *Journal of Ethnopharmacology*, 97(2), pp.293–299. https://doi.org/10.1016/j.jep.2004.11.014.

Ying, S., Guan, Z., Ofoegbu, P.C., Clubb, P., Rico, C., He, F. and Hong, J., 2022. Green synthesis of nanoparticles: Current developments and limitations. *Environmental Technology & Innovation*, 26, p.102336. https://doi.org/10.1016/j.eti.2022.102336.

Zakaria, Z.A., Hassan, M.H., Nurul Aqmar, M.N.H., Abd Ghani, M., Mohd Zaid, S.N.H., Sulaiman, M.R., Hanan Kumar, G. and Fatimah, C.A., 2007. Effects of various nonopioid receptor antagonists on the antinociceptive activity of Muntingia calabura extracts in mice. *Methods and Findings in Experimental and Clinical Pharmacology*, [online] 29(8), pp.515–520. https://doi.org/10.1358/mf.2007.29.8.1119164.

APPENDICES

Appendix A

Calculation for band gap energy, E_{bg}:

$$E_{bg} = \frac{hc}{\lambda}$$

$$= \frac{(6.626 \times 10^{-34}\ \text{Js})\ (3.0 \times 10^{8}\ ms^{-1})}{3.73 \times 10^{-7} m}$$

$$= 5.329 \times 10^{-19}\ \text{J}$$

Given that 1 eV = 1.602×10^{-19} J

Hence, 5.329×10^{-19} J = 3.32 eV

Where,

h = Planck's constant (6.626×10^{-34} Js)

c = Speed of light (3.00×10^{8} ms^{-1})

λ = Maximum absorption wavelength (373 nm)

Appendix B

Crystallite size of synthesized ZnO NPs

Calculation for β

$$\beta = \frac{\text{FWHM in } 2\theta \times \pi}{180^\circ}$$

$$= \frac{0.20 \times \pi}{180^\circ}$$

$$= 3.491 \times 10^{-3}$$

Calculation for crystallite size by Debye-Scherrer Equation

$$D = \frac{K\lambda}{\beta \cos\theta}$$

$$= \frac{(0.9)\,(1.5406 \times 10^{-10}\text{m})}{3.491 \times 10^{-3} \cos\,(15.96)}$$

$$= 4.13 \times 10^{-8}\,\text{m}$$

$$= 41.3\ \text{nm}$$

Where,

D = Crystallite size in diameter

K = Scherrer constant, 0.9

λ = Wavelength of X-ray source (Cu K_α radiation= 1.5406 Å)

β = Full width at half maximum (FWHM) of the diffraction peak in radian 2θ

θ = Bragg's angle of diffraction

The similar calculation was performed to calculate for the rest of the matched peaks to obtain an average value of crystallite size as shown in the table below:

Table: Calculation of the average crystallite size.

2θ	FWHM (°)	θ	β(radians)	D (nm)
31.92	0.20	15.96	0.00349	41.31
34.58	0.20	17.29	0.00349	41.60
36.41	0.16	18.21	0.00279	52.27
47.70	0.16	23.85	0.00279	54.29
56.75	0.16	28.38	0.00279	56.43
63.02	0.20	31.51	0.00349	46.59
66.53	0.16	33.27	0.00279	59.38
68.11	0.24	34.06	0.00419	39.95
69.25	0.20	34.63	0.00349	48.27
			Average	48.90

Appendix C

*** Basic Data Process ***

Group : Standard
Data : CJM_ZM6

Strongest 3 peaks

no.	peak no.	2Theta (deg)	d (A)	I/I1	FWHM (deg)	Intensity (Counts)	Integrated Int (Counts)
1	6	36.3304	2.47083	100	0.21720	88678	1073134
2	3	31.8329	2.80890	60	0.20230	53593	596229
3	5	34.4946	2.59801	57	0.18120	50250	536647

Peak Data List

peak no.	2Theta (deg)	d (A)	I/I1	FWHM (deg)	Intensity (Counts)	Integrated Int (Counts)
1	28.6852	3.10957	15	0.21240	12969	155527
2	31.0696	2.87615	13	0.19230	11275	125032
3	31.8329	2.80890	60	0.20230	53593	596229
4	32.6990	2.73645	27	0.18860	24031	271541
5	34.4946	2.59801	57	0.18120	50250	536647
6	36.3304	2.47083	100	0.21720	88678	1073134
7	42.7832	2.11191	8	0.15190	7120	64220
8	47.6220	1.90800	21	0.21770	19039	234249
9	50.7947	1.79602	12	0.15520	10504	98876
10	56.3048	1.63262	12	0.17370	10507	105168
11	56.6745	1.62284	32	0.19820	28184	293650
12	56.9200	1.61643	4	0.07600	3337	23921
13	60.7355	1.52369	9	0.16780	7666	77504
14	61.7275	1.50156	4	0.16660	3885	41153
15	62.9540	1.47523	28	0.22500	24875	327852
16	66.4666	1.40553	5	0.18320	4459	49097
17	68.0385	1.37684	23	0.21690	20477	236530
18	68.2800	1.37255	3	0.10200	2908	31405
19	69.1803	1.35687	13	0.18930	11723	135371

Figure: XRD information of synthesized ZnO NPs (Part I).

Appendix D

```
        ***  Basic Data Process  ***

# Data Infomation
          Group                : Standard
          Data                 : CJM_ZM6
          Sample Nmae          : ZM6
          Comment              :
          Date & Time          : 03-04-24 13:33:20

# Measurement Condition
    X-ray tube
          target               : Cu
          voltage              : 40.0 (kV)
          current              : 30.0 (mA)
    Slits
          Auto Slit            : not Used
          divergence slit      :   1.00000 (deg)
          scatter slit         :   1.00000 (deg)
          receiving slit       :   0.30000(mm)
    Scanning
          drive axis           : Theta-2Theta
          scan range           :   10.0000 - 70.0000 (deg)
          scan mode            : Continuous Scan
          scan speed           :    0.5000 (deg/min)
          sampling pitch       :    0.0200 (deg)
          preset time          :    2.40 (sec)

# Data Process Condition
    Smoothing                  [ AUTO ]
          smoothing points     : 11
    B.G.Subtruction            [ AUTO ]
          sampling points      : 15
          repeat times         : 30
    Ka1-a2 Separate            [ MANUAL ]
          Ka1 a2 ratio         : 50 (%)
    Peak Search                [ AUTO ]
          differential points  : 11
          FWHM threhold        : 0.050 (deg)
          intensity threhold   : 30 (par mil)
          FWHM ratio  (n-1)/n  : 2
    System error Correction    [ NO ]
    Precise peak Correction    [ NO ]
```

Figure: XRD information of synthesized ZnO NPs (Part II).

Appendix E

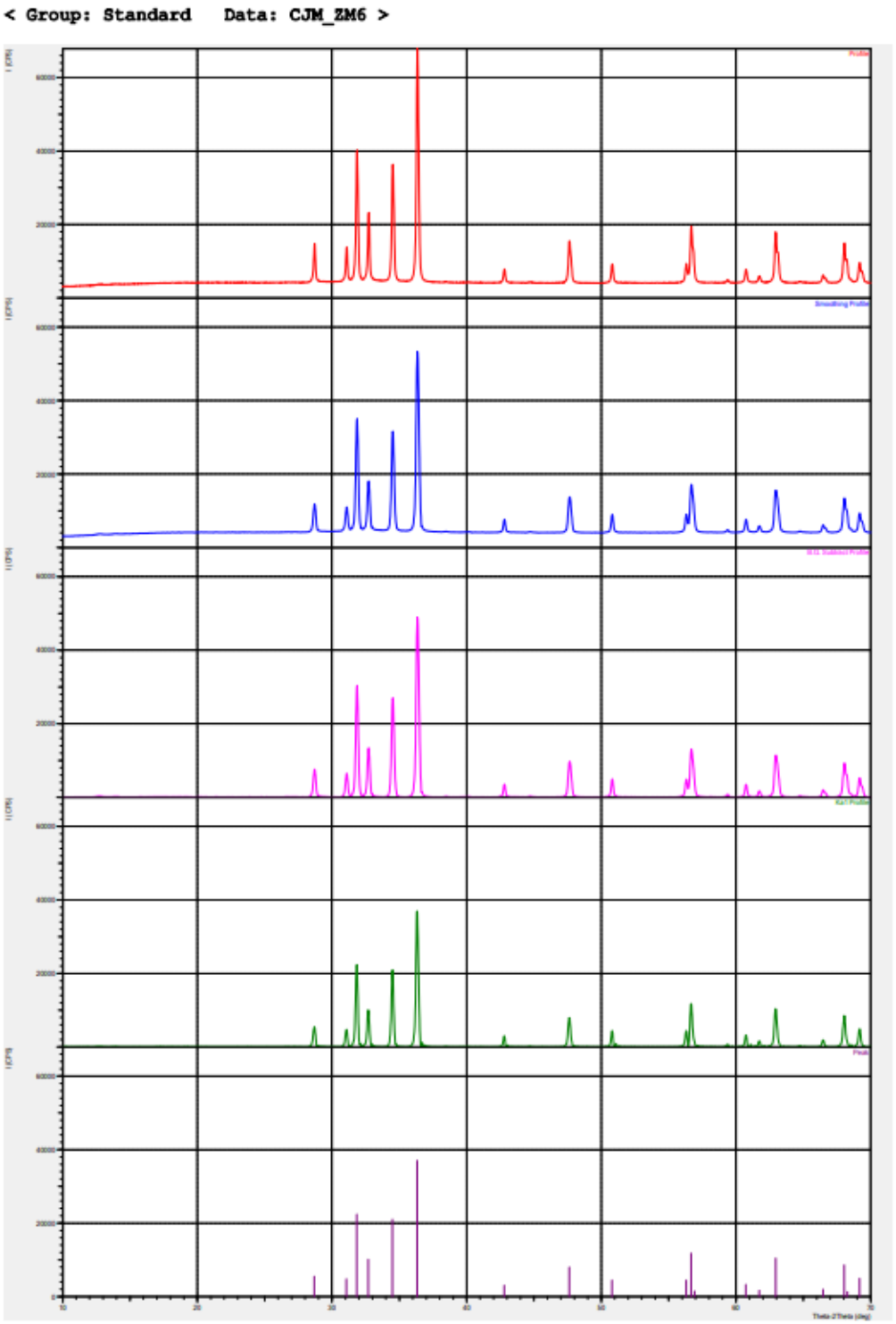

Figure: XRD information of synthesized ZnO NPs (Part III).

Appendix F

Match! Phase Analysis Report

Universiti Tunku Abdul Rahman, Faculty of Science

Sample: ZM6 ()

Sample Data	
File name	CJM_ZM6.RAW
File path	C:/xddat/Standard/CJM_ZM6
Data collected	Mar 4, 2024 15:35:34
Data range	10.060° - 70.060°
Original data range	10.000° - 70.000°
Number of points	3001
Step size	0.020
Rietveld refinement converged	No
Alpha2 subtracted	No
Background subtr.	No
Data smoothed	No
2theta correction	0.06°
Radiation	X-rays
Wavelength	1.540600 Å

Matched Phases

Index	*Amount (%)*	*Name*	*Formula sum*
A	87.8	Zinc Oxide Zincite, syn	Zn O
	12.2	*Unidentified peak area*	

A: Zinc Oxide Zincite, syn (87.8 %)	
Formula sum	Zn O
Entry number	01-071-6424
Figure-of-Merit (FoM)	0.932745
Total number of peaks	27
Peaks in range	9
Peaks matched	9
Intensity scale factor	1.08
Space group	P63mc
Crystal system	hexagonal
Unit cell	a= 3.2494 Å c= 5.2038 Å
I/Ic	5.21
Calc. density	5.680 g/cm³
Reference	Kihara, K., Donnay, G., Can. Mineral. **23**, 647 (1985)

Candidates

Name	*Formula*	*Entry No.*	*FoM*
Zinc Gallium Phosphide Borate	(Zn6 Ga2) P2 (B O2)12	01-082-0082	0.7378
Zinc Indium Iron Oxide	In Fe Zn6 O9	00-040-0247	0.7040
Zinc Indium Iron Oxide	In Fe Zn5 O8	00-040-0246	0.6737
Copper Zinc Phosphate Hydrate	(Cu0.81 Zn0.19)3 (P O4)2 H2 O	00-059-0626	0.6695
Zinc Indium Iron Oxide	In Fe Zn4 O7	00-040-0245	0.6663
Zinc Arsenate	Zn2 As2 O7	00-001-0798	0.6589
Zinc Gallium Oxide	Zn0.907 Ga0.186 O1.186	00-048-0484	0.6582
Zinc Oxide	Zn O	01-077-9355	0.6474
Copper Iron Nickel Zinc Oxide	Cu0.6 Fe1.4 Ni0.65 Zn0.35 O4	00-048-0492	0.6469
Zinc Gallium Scandium Oxide	Sc Ga Zn5 O8	00-040-0274	0.6462
Zinc Gallium Oxide	Zn9 Ga2 O12	00-050-0448	0.6446
Silver Zinc Phosphate	Ag2 Zn (P2 O7)	01-070-4459	0.6396
Potassium Zinc Silicate	K2 Zn (Si O4)	01-087-1488	0.6380
Selenide Zinc Oxide	Se (Zn O3)	01-077-9203	0.6365
Sodium Iron Zinc Phosphate Hydrate	Na - Fe - Zn - P O4 - H2 O	00-030-1207	0.6362
Sodium Iron Zinc Phosphate Hydrate	Na - Fe - Zn - P O4 - H2 O	00-032-1106	0.6362
Tin Zinc Titanium Zirconium Oxide	Zn ((Zn (Ti0.5 Sn0.5)0.75 Zr0.25) O4)	01-076-7224	0.6338
Zinc Selenite	Zn (Se O3)	01-070-0245	0.6337
Tin Zinc Titanium Zirconium Oxide	Zn ((Zn (Ti0.5 Sn0.5)0.7 Zr0.3) O4)	01-076-7225	0.6306
Sodium Calcium Magnesium Strontium Zinc Aluminum Iron Manganese Titanium Silicate (Gehlenite, sodian, strontian)	(Ca0.84 Sr0.45 Na0.71) (Mg0.19 Fe0.29 Mn0.03 Zn0.02 Al0.46 Ti0.01) ((Si1.99 Al0.01) O7)	01-076-2565	0.6280
Sodium Calcium Magnesium Strontium Zinc Aluminum Iron Manganese Titanium Silicate (Gehlenite, sodian, strontian)	(Ca0.83 Sr0.45 Na0.72) (Mg0.20 Fe0.29 Mn0.03 Zn0.01 Al0.45 Ti0.02) ((Si1.99 Al0.01) O7)	01-076-2566	0.6276
Calcium Zinc Praseodymium Titanium Oxide	Ca Pr2 Zn Ti2 O9	00-056-0389	0.6266
Zinc Lead Oxide	Znx Pb1-x O	00-023-1497	0.6244
Copper Zinc Selenium Oxide	(Cu0.5 Zn0.5) (Se O3)	01-072-4737	0.6219
Zinc Arsenate	Zn2 As2 O7	01-079-8176	0.6201
Zinc Gallium Oxide	Zn (Ga2 O4)	01-084-3649	0.6196
Zinc Antimony Oxide	Zn (Zn1.36 Sb0.64) O4	01-074-8075	0.6193
Copper Zinc Selenium Oxide	(Cu0.2 Zn0.8) (Se O3)	01-072-4740	0.6189
Zinc Cadmium Tin Oxide	Zn.8 Cd1.2 Sn O4	01-074-2190	0.6189

Figure: XRD information of synthesized ZnO NPs matching with ICDD card No. 01-071-6424 (Part I).

Appendix G

Tin Zinc Titanium Zirconium Oxide	Zn ((Zn (Ti0.5 Sn0.5)0.8 Zr0.2) O4)	01-076-7223	0.6181
Zinc Arsenate	Zn2 As2 O7	00-051-1601	0.6168
Zinc Cerium Oxide	(Ce0.97 Zn0.03) O2	01-075-8372	0.6122
Zinc Antimony Oxide	(Zn7 Sb2 O12)0.333	01-075-6982	0.6097
Calcium Zinc Neodymium Titanium Oxide	Ca Nd2 Zn Ti2 O9	00-056-0390	0.6076
Zinc Cerium Oxide	(Ce0.97 Zn0.03) O2	01-075-8373	0.6076
Potassium Zinc Phosphate	K6 Zn (P2 O7)2	00-033-1005	0.6075
Calcium Zinc Lanthanum Manganese Oxide	(La0.667 (Ca0.2 Zn0.8)0.333) (Mn O3)	01-082-8255	0.6051
Zinc Lead Oxide	Zn Pb O3	00-023-1498	0.6038
Zinc Cadmium Tin Oxide	Zn.4 Cd1.6 Sn O4	01-074-2192	0.6027
Tin Zinc Titanium Zirconium Oxide	Zn ((Zn (Ti0.667 Sn0.333)0.7 Zr0.3) O4)	01-076-7229	0.6026

Search-Match

Settings

Reference database used	PDF-2 Release 2016 RDB
Automatic zeropoint adaptation	Yes
Minimum figure-of-merit (FoM)	0.60
2theta window for peak corr.	0.30 deg.
Minimum rel. int. for peak corr.	1
Parameter/influence 2theta	0.50
Parameter/influence intensities	0.50
Parameter multiple/single phase(s)	0.50

Selection Criteria

Elements:

Elements that must be present: O, Zn

Elements that may be present: All elements not mentioned above

Peak List

No.	*2theta [°]*	*d [Å]*	*I/I0*	*FWHM*	*Matched*
1	28.77	3.1006	150.54	0.1200	
2	31.15	2.8685	130.24	0.1600	
3	31.92	2.8013	547.74	0.2000	A
4	32.79	2.7288	267.97	0.1600	
5	34.58	2.5917	490.98	0.2000	A
6	36.41	2.4655	1000.00	0.1600	A
7	42.86	2.1081	55.06	0.1600	
8	47.70	1.9051	173.21	0.1600	A
9	50.87	1.7934	75.71	0.1600	
10	56.38	1.6306	74.73	0.2000	
11	56.75	1.6209	230.32	0.1600	A
12	56.92	1.6164	120.79	0.1600	
13	59.44	1.5538	11.29	0.1200	
14	60.81	1.5220	52.90	0.1600	
15	61.80	1.5001	25.43	0.2000	
16	63.02	1.4739	208.03	0.2000	A
17	63.20	1.4701	115.41	0.2400	
18	66.53	1.4043	31.76	0.1600	A
19	66.74	1.4004	16.99	0.2000	
20	68.11	1.3756	160.48	0.2400	A
21	68.30	1.3722	92.86	0.2000	
22	69.25	1.3558	80.85	0.2000	A
23	69.44	1.3524	45.75	0.2000	

Rietveld Refinement using FullProf

Calculation was not run or did not converge.

Crystallite Size Estimation using Scherrer Formula

Calculation was not run.

Degree of crystallinity analysis

Profile area	*Counts*	*Amount*
Total area	36446372	100.00%
Diffraction peaks	6731429	18.47%
Background	29714943	81.53%
Instrumental background	1734077	4.76%
Amorphous phases	27980865	76.77%

Degree of crystallinity (DOC) = 19.39%
Amorphous content (weight %) =80.61%

Figure: XRD information of synthesized ZnO NPs matching with ICDD card No. 01-071-6424 (Part II).

Appendix H

Integrated Profile Areas

Based on calculated profile

Profile area	*Counts*	*Amount*
Overall diffraction profile	36446372	100.00%
Background radiation	29714943	81.53%
Diffraction peaks	6731429	18.47%
Peak area belonging to selected phases	2283284	6.26%
Peak area of phase A (Zinc Oxide Zincite, syn)	*2283284*	*6.26%*
Unidentified peak area	4448146	12.20%

Peak Residuals

Peak data	*Counts*	*Amount*
Overall peak intensity	144918	100.00%
Peak intensity belonging to selected phases	136026	93.86%
Unidentified peak intensity	8892	6.14%

Diffraction Pattern Graphics

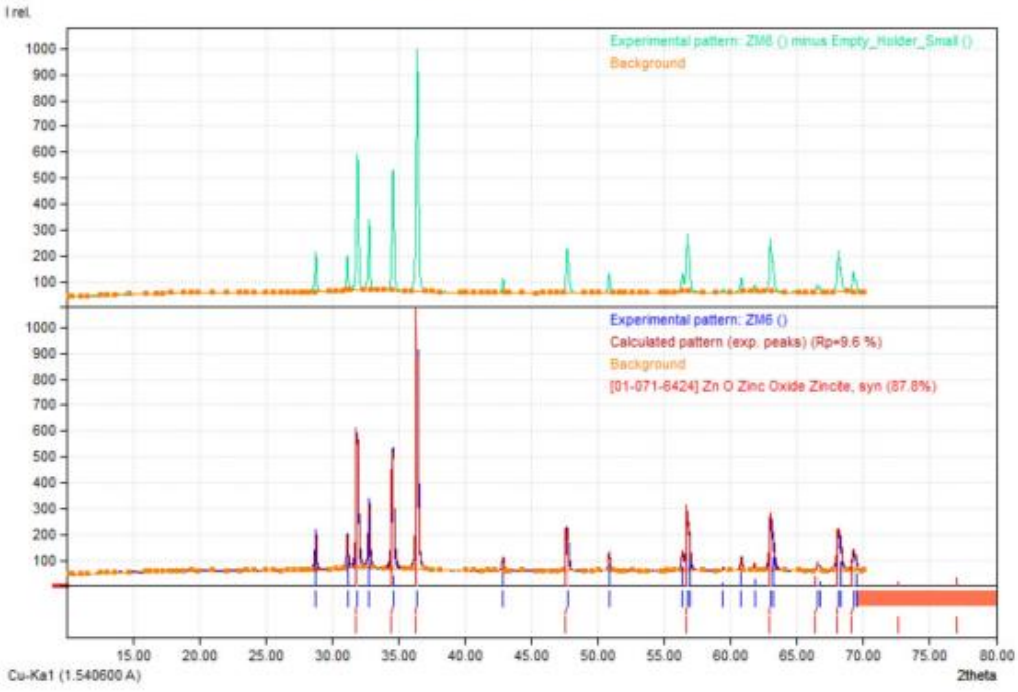

Figure: XRD information of synthesized ZnO NPs 87.8% matching with ICDD card No. 01-071-6424 (Part III).